Numerical modelling of overriding plate deformation and slab rollback in the Western Mediterranean

Master Thesis
Luuk Schuurmans

Supervised by Menno Fraters & dr. Wim Spakman

Sunday 1st July, 2018

Abstract

In the Western Mediterranean, rollback of the Calabrian slab resulted in a two-phase opening of the Liguro-Provençal Basin (30-16 Ma) and the Tyrrhenian Basin (9 Ma-present), with a transient quiet period in between. The cause of the discontinuous opening of these basins is not well understood, as well as the cause for the subduction to jump from the western to the eastern side of Corsica and Sardinia at the onset of extension in the Tyrrhenian Basin, leaving the Corsica/Sardinia block behind. In this study the cause of this stagnation and reactivation of rollback is investigated using 2D numerical modelling with ASPECT. To study the controlling factors on opening of the Liguro-Provençal Basin and the Tyrrhenian Basin, modelling of a central transect through the two back-arc domains is performed. The focus is on the effect of lithospheric strength, absolute plate motions and pre-existing weak zones on the evolution of overriding plate deformation. The results of the numerical models are compared to the existing geological framework. The presence and strength of weak zones seems to play a major role in the evolution of overriding plate deformation, as well as the total amount of rollback. Simulating the stagnation and reactivation of rollback has proven to be challenging in 2D due to the geometry of the narrow Calabria slab. Toroidal flow around the slab edges plays a major role on the evolution of overriding plate deformation and the rates of back-arc extension. Furthermore, the strength of the material in the weak zones is an important controlling factor for back-arc extension rates.

Contents

1 Introduction

Subduction is one of the main driving processes of plate tectonics on Earth. The interplay of slab geometry and velocity boundary conditions in subduction zones plays a large role in the evolution of overriding plate deformation and the formation of back-arcs (e.g. Doglioni (1991); Hassani et al. (1997). While back-arc extension due to slab rollback is present in multiple regions on Earth, there are some regions where the opening of a back-arc basin is a discontinuous process, like the Lau Basin (Hawkins, 1995), the Philipine Sea Basin (Seno and Maruyama, 1984) and the Western Mediterranean (Dewey et al., 1989). The cause of this discontinuous opening is still unknown, and will be the focus of this study. The Western Mediterranean is a good example of a region which has been influenced a lot by the evolution of a subduction system. In the last 30 million years, two separate stages of rollback of the Calabrian slab with a stagnation stage in between have determined the present day geometry of the Western Mediterranean. While the kinematic history of the area has been studied extensively, it is still uncertain what the cause of the rollback stagnation is. Faccenna et al. (2001) proposed that the slab tip arrival at the 660 km discontinuity is a key factor in decreasing the subduction rate and trench migration velocity. At the time the slab tip arrives at the impermeable boundary with a viscosity and density jump, it cannot immediately sink further and folding into a horizontal position is the only possible motion for the slab (Faccenna et al., 2001). At the time the bottom part of the slab lies on the 660 discontinuity, trench retreat can continue, resulting in the formation of the Tyrrhenian basin during the second stage of rollback. The validity of the proposed mechanism of Faccenna et al. (2001) will be tested by simulating the rollback history of the Calabrian slab in the Western Mediterranean. A 2D numerical model performed with the finite element geodynamical code ASPECT Heister et al. (2017) will be executed to study the effect of upper plate rheology, boundary conditions and slab dynamics on rollback stagnation and episodic back-arc extension.

1.1 Geological setting

In this study, there will be a focus on simulating the geological history and setting of the Western Mediterranean using a 2D numerical model. The Western Mediterranean area comprises the area between the mainland of Spain, France, Italy and North-Africa and is formed by relative movements of micro-continental blocks and the African and European plates. The region has proven to be an interesting area for investigating subduction and consequential rollback and back-arc extension in an overall convergent setting (e.g. Mantovani et al. (1996); Wortel and Spakman (2000)). The tectonic evolution of the Western Mediterranean has been studied extensively, resulting in well constrained geological and kinematic reconstructions (Dewey et al., 1989; Doglioni et al., 1997; Faccenna et al., 2004; Spakman and Wortel, 2004; van Hinsbergen et al., 2014).

The Western Mediterranean region underwent a complex geological history. The area is located in a convergent tectonic setting, caused by the relative movement between Africa and Europe (e.g.Gaina et al. (2013)). Prior to the onset of Africa-Europe

convergence around 85 Ma, a 35°counterclockwise rotation of Iberia with respect to Europe occurred. The timing of this rotation is restricted to the Aptian (125-112 Ma) based on sea-floor spreading data from the Bay of Biscay (Gong et al., 2008), which was confirmed by Vissers and Meijer (2012) who proposed a rotation between 121 and 112 Ma. The Africa-Iberia motion during this period is difficult to constrain due to the absence of magnetic anomalies on the seafloor during the Cretaceous Normal Superchron (121 - 84 Ma). However, using the relative Iberia-Europe and Africa-North America motions, one can assume that a strike slip fault was present between Africa and Iberia (Dewey et al., 1973). Plate reconstruction from ocean magnetic anomalies in the area do not allow for any convergence between Iberia and Africa during the Cretaceous Normal Superchron from 121 until 84 Ma (van Hinsbergen et al., 2014). Instead, Africa's motion with respect to Europe was one of sinistral strike slip, which is in correspondence with the separation of Africa and North America during the opening of the Central Atlantic Ocean (Dewey et al., 1989). Since no convergence between Africa and Europe occurred before 84 Ma, all convergence is constrained to the last 84 million years. Convergence rates slowly increased from 84 Ma onwards (Kley and Voigt, 2008). Most of the Africa-Europe convergence took place in the last 45 My, and therefore it is unlikely that a slab has formed below Iberia before 45 Ma (van Hinsbergen et al., 2014). Between 45 and 30 Ma, convergence between Africa and Europe was an ongoing process, including the formation of a slab beneath Corsica and Sardinia. The total amount of convergence between Africa and Europe between 65 Ma and 35 Ma at the position of Sardinia is estimated to be 250 km (van Hinsbergen et al., 2014). Additional information from arc volcanism around 38 Ma at Sardinia and the Provence (Lustrino et al., 2009) indicate that the slab had reached a depth of approximately 100-150 km at that time. Besides this constraint from arc volcanism, there is also evidence that a part of the convergence between Africa and Europe was accommodated in the Provence in Eocene time (Lacombe and Jolivet, 2005). The total amount of shortening in the Provence area is determined to be 15-20 km, but the total amount of convergence stored in the Liguro Provençal basin and the Western Alps is still unknown. Besides, there are still uncertainties on the distribution of the convergence between the subducting slab and shortening in the Provence. Therefore, the slab length below Sardinia during incipient rollback is unknown. In the model in this study, an initial slab length of 250 km is used, which is based on the total amount of Africa-Europe convergence between 65 Ma and 35 Ma.

At 30 Ma, the total slab length beneath the Corsica and Sardinia block and its resulting negative buoyancy was sufficient to initiate rollback (van Hinsbergen et al., 2014). This rollback caused rifting of the continental domain on the overriding plate. The temporal evolution of the rollback and back-arc extension of the Western Mediterranean is shown in figure 1. While there are two common explanations for the origin of the Corsica-Sardinia block, they both agree on the fact that it was separated from the European mainland by a pre-existing weaker zone (Stampfli et al., 2002; Rosenbaum et al., 2002b; Advokaat et al., 2014). Stampfli et al. (2002) proposed that the Corsica-Sardinia block was part of rigid Iberia, and that the Valais suture zone was connected to the Bay of Biscay. This suture would then act as the weak zone between the Corsica-Sardinia block and the European mainland. On the other hand Rosenbaum

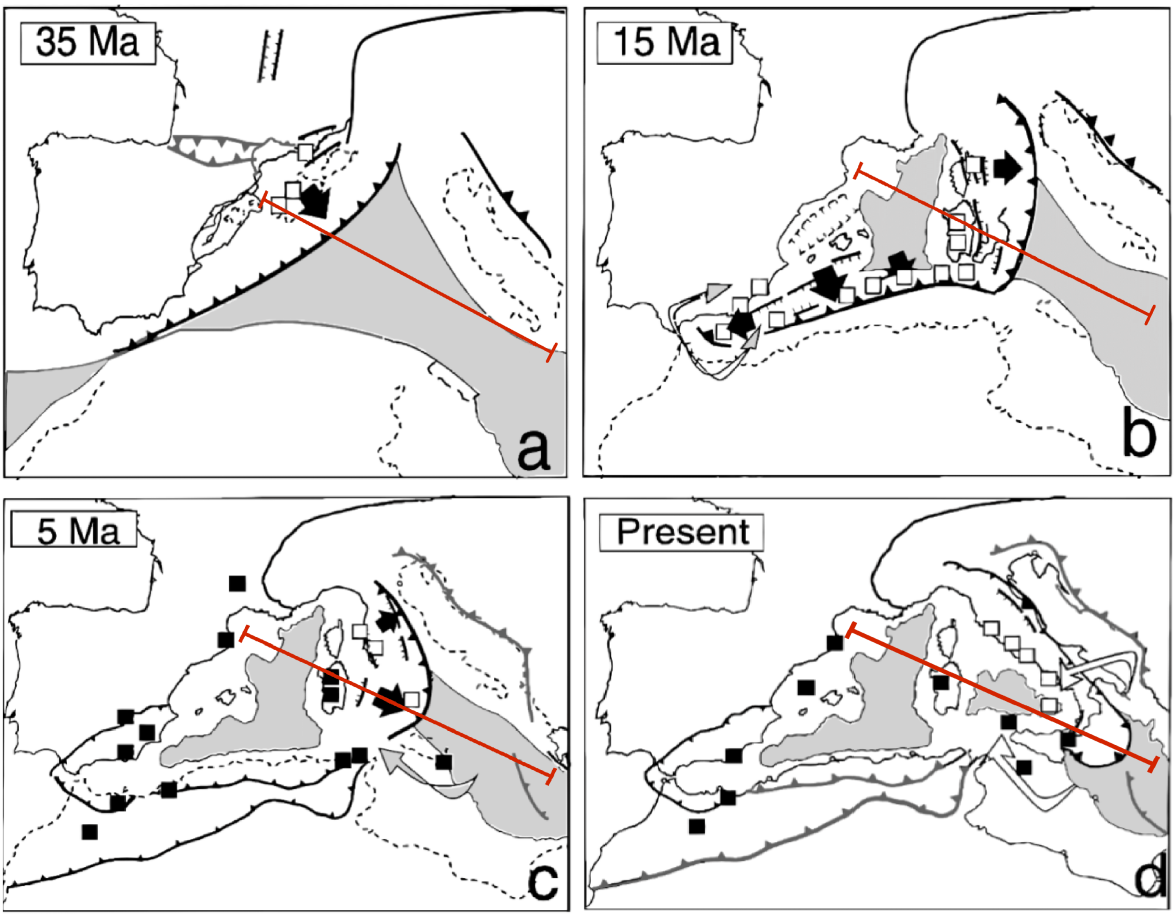

Figure 1: Temporal evolution of the geological setting in the Western Mediterranean. The 2D cross section of this study is made along the red line. Figure adjusted from Faccenna et al. (2004).

et al. (2002a) proposed that Corsica and Sardinia were disconnected from rigid Iberia since they experienced rotations at different time. This theory is endorsed with paleomagnetic evidence by Advokaat et al. (2014). However, in both theories a weak zone in the form of a suture or plate boundary is present north of the Corsica and Sardinia block to accommodate the onset of overriding plate extension. Therefore the implementation of a weak zone in the model is a prerequisite, independent of the choice of the governing model.

During slab rollback, subduction-related calc-alkaline volcanism in the Provence and on Sardinia was active (Girod and Girod, 1977). Since this volcanism was a result of the north-/northwestward dipping Calabrian slab, the intra-continental rifting on the overriding plate can be interpreted as back-arc extension (Rehault et al., 1984). Rollback of the Calabrian slab resulted in the opening of the Liguro Provençal basin from 30 Ma until 16 Ma (Séranne, 1999; Chamot-Rooke et al., 1999). Rifting in the Liguro Provençal basin continued until 21 Ma, after which oceanic crust was formed from 21 Ma until 16 Ma (Burrus, 1984). This episode of oceanic crust formation was

accompanied by the rotation of Sardinia, which took place within a short time span between 20.5 Ma and 19 Ma (Montigny et al., 1981).

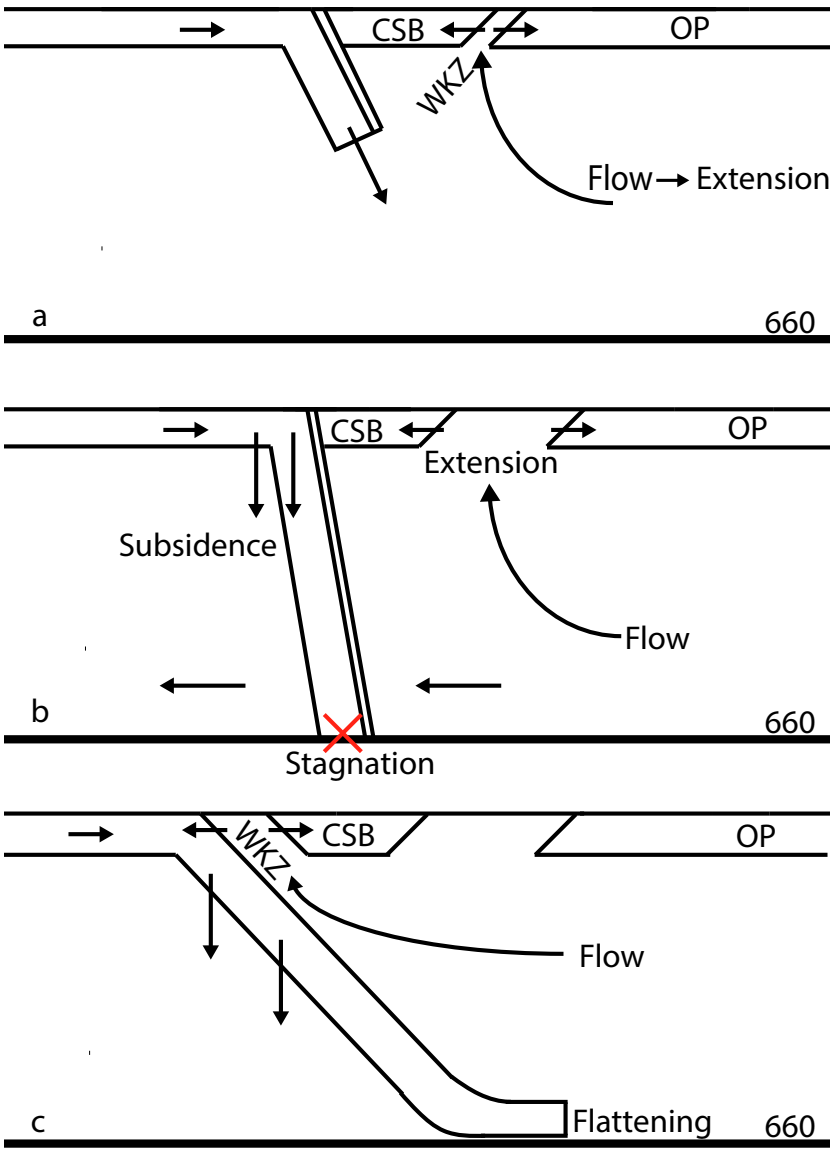

Figure 2: Schematic representation of the hypothesis for rollback stagnation proposed by Faccenna et al. (2001). a) Rollback initiation and first stage of back-arc extension; b) Stagnation of the slab tip on the 660 km discontinuity, subsidence of the slab hinge; c) Rollback restarts, second stage of back-arc extension. WKZ= Weak Zone, OP = Overriding plate, CSB = Corsica-Sardinia Block

Around 16 Ma, a stagnation of slab rollback occurred in the Western Mediterranean (e.g. Rosenbaum et al. (2002b). The exact cause of this stagnation period is still unknown, and will be the focus of this study. Figure 2 is a schematic representation of the hypothesis as proposed by Faccenna et al. (2001) which will be tested in this study. During the first stage (figure 2a), the negative buoyancy of the slab causes it to

initiate rollback. As a result, extension is initiated in the weakest zone of the overriding plate, which is the weak zone between the Corsica-Sardinia block and the overriding plate (the European mainland). When rollback progresses, deformation is still localized in the weakest zone and back-arc extension continues creating the Liguro Provençal basin. The Corsica-Sardinia block is still attached to the slab, preventing hot mantle material to flow in between the slab and the continental block. After reaching the 660 km discontinuity, the slab tip of the Calabrian slab cannot immediately sink further because of a viscosity jump and a phase change at the transition to the lower mantle, causing a stagnation of the rollback process. This results in subsidence around the hinge point of the slab, creating space between the slab and the Corsica-Sardinia block. Hot mantle material can flow in this zone creating a new zone for localized deformation, and a new extensional region can be developed between the Corsica-Sardinia Block and Calabria, which is still attached to the slab. This extensional period corresponds to the formation of the Tyrrhenian basin (e.g. Malinverno and Ryan (1986)). The slab tip that stagnated on the 660 km discontinuity is now horizontally draped on top of it. The Calabrian slab is a good example of a continuous slab which is confined to the upper mantle, as proven with tomographic images (Spakman and Wortel, 2004). As can be seen in figure 3, the slab sinks sub-vertically in the upper mantle and is flat lying on the 660 km boundary between the upper and lower mantle at present.

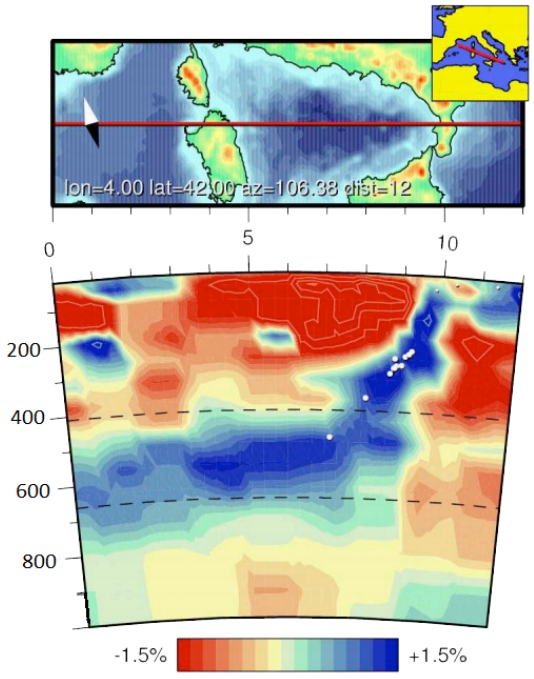

Figure 3: Tomographic cross section through the Tyrrhenian mantle and Calabria. The dashed lines indicate the 410 and 660 km mantle discontinuities. The red line on the map-inset indicates the location of the cross-section, which roughly corresponds to the model domain of this study. Figure from Spakman and Wortel (2004)

After the phase of rollback stagnation between 16 and 10 Ma, a slab tear occurred in the Sicily channel, which resulted in a narrowing of the Calabria slab (Faccenna et al., 2004). The Calabrian block was still attached to the Calabrian slab and continued its rollback. However, the Calabrian block shows a partly similar tectonic history and nappe sequence as the Northeastern part of Corsica (Alvarez et al., 1974). This supports the idea that Calabria initially was part of the Corsica-Sardinia block before it was detached and moved southeastwards. Opening of the Tyrrhenian Basin and the detachment of the Calabria block from the Corsica-Sardinia block started around 10 Ma, and was the result of arc migration, as first proposed by Malinverno and Ryan (1986). The Corsica-Sardinia block was already brought to its current position before the rollback stagnation period, and was not affected by this second stage of rollback. The velocity of slab rollback resulting in the detachment of Calabria and the formation of the Tyrrhenian basin was relatively high compared to rollback rates of surrounding slabs (Rosenbaum and Lister, 2004). This higher velocity can possibly be explained by the width of the slab. Dvorkin et al. (1993) showed that slab sinking rates can increase rapidly when a slab is narrow, due to toroidal flow of asthenospheric material around the slab edges. The formation of slab windows on both edges of the Calabrian slab is accommodated by Subduction-Transform Edge Propagator (STEP) faults (Govers and Wortel, 2005).

The back-arc extension in the overriding plate crust resulted in thinning of the continental crust, and at some places even oceanic crust formed. The interplay of the rollback history of the Calabrian slab and the formation of these marine basins, which have been formed since the Oligocene, have been the subject of many studies (e.g. Séranne (1999), Faccenna et al. (2001) and Faccenna et al. (2004)). Both the Liguro Provençal Basin and the Tyrrhenian Basin comprise partly of oceanic crust. In the Liguro Provençal basin, the oceanic crust is distributed as a continuous patch, where the Tyrrhenian Basin contains two areas of oceanic crust (the Vavilov and Marsili basins) separated by a sill called the Issel bridge (Sartori et al., 1990). The grey colours in figure 1 indicate the areas with oceanic crust. The presence of oceanic crust indicates that extensive back-arc extension has taken place in both the Liguro Provençal Basin and the Tyrrhenian Basin. This extension finally resulted in continental break-up and subsequent oceanic spreading, instead of thinning of continental crust only. In the model runs of this study, the formation of oceanic crust will be attempted to simulate.

The main aim of this study is to investigate different numerical model set ups regarding boundary conditions and overriding plate rheology that lead to subduction rollback model that possibly can explain the geological history of the Western Mediterranean, with an emphasis on the stagnation period in slab rollback between 16 and 10 Ma and the current state of the slab. A 2D cross section through the domain will be made, perpendicular to the strike of the slab. The location of the cross section is indicated in figure 1 by the red line. The governing boundary conditions that are implemented in this study will be discussed in the following sections.

2 ASPECT

ASPECT (Kronbichler et al., 2012; Heister et al., 2017) is a finite element code written in C++. The code is designed to simulate geodynamic processes like mantle convection and subduction in the Earth. Like most geodynamical codes, ASPECT solves the Stokes and the temperature equations, which describe thermally driven convection. To do this, the material in the Earth is assumed to be a highly viscous fluid. Using this assumption the laws of continuum mechanics for fluids can be applied to the Earth. In this formulation some fundamental physical laws like the conservation of momentum, energy and mass can be applied. In the following section I will elaborate on the code structure, the basic equations and applications of ASPECT for this study.

2.1 Code structure

ASPECT is a code which is built in a very structured way. The main code is based on the following main principles (Bangerth et al., 2017):

- *Usability and extensibility*
  The code of ASPECT is built in such a way that it can be extended with plugins for different models and set-ups in an easy way. This opens up the possibility to use the code for varying applications.

- *Modern numerical methods*
  ASPECT uses numerical methods that are very modern and developed. Examples are the use of adaptive mesh refinement, non-linear solvers and stabilization of transport-dominated processes. These modern methods cause the solutions to be highly accurate and efficient in CPU usage.

- *Parallelism*
  Computations for the different setups for this study are executed for a large domain. To solve this problems, a lot of computational power is needed, which can not be provided by a single computer. ASPECT is designed in such a way that it works in a massively parallel way, which means that a large amount of processors work together to achieve the solution.

- *Building on others' work*
  The code of ASPECT builds upon existing libraries of codes. The three main libraries ASPECT builds on are DEAL.II, Trilinos and p4est. DEAL.II (Arndt et al. (2017)) is responsible for everything that has to do with the construction of the finite elements, geometries and meshes. Trilinos (Heroux et al. (2005)) is used to perform parallel linear algebra calculations, while p4est (Burstedde et al. (2011)) is needed for parallel mesh handling.

ASPECT itself consists of a small core code and many plugins, which are invoked by the core code. The core code is responsible for solving the basic equations, while the separate plugins are invoked to exert a certain part of the work in the model. Due to

this separation of core code and plugins one can easily use ASPECT in many different applications.

An example of such a plugin is the material model plugin. Many material models are available in the ASPECT intrinsic code, and for each setup the user can define the required material model. To prevent repeatedly recompiling of the code for different setups of the model, ASPECT uses an external input parameter file. This parameter file contains all the information for a single model run, and passes the necessary information to the core of the code to invoke the correct plugins. The parameter file is structured in such a way that different parts of the model are declared in different subsections, while global parameters such as dimension and solver tolerances are defined outside the subsections. In the subsections the user can assign values to parameters manually, but it is also possible to use the default value of the parameters which is implemented in the plugins itself. The use of an user-friendly external parameter file makes it very easy to adjust run time parameters for different models. Figure 4 shows an example of a part of an input parameter file, with the global parameters on top, and the local parameters declared in the subsections.

```
set Dimension                              = 2
set End time                               = 30e6
set CFL number                             = 0.1
set Timing output frequency                = 0
set Use years in output instead of seconds = true
set Maximum time step                      = 1000
set Output directory                       = iofiles/subduction/viscoplastic/open/open37/output
set Nonlinear solver scheme                = iterated Stokes
set Max nonlinear iterations               = 50
set Nonlinear solver tolerance             = 1e-5
set Linear solver tolerance                = 1e-5
set Temperature solver tolerance           = 5e-12
set Number of cheap Stokes solver steps    = 200
set Pressure normalization                 = no
set Resume computation                     = auto

subsection Geometry model
  set Model name = box with lithosphere boundary indicators
    subsection Box with lithosphere boundary indicators
      set Lithospheric thickness    = 100000
      set X repetitions             = 10
      set Y repetitions             = 5
      set X extent                  = 24e5
      set Y extent                  = 76e4
     end
end

subsection Gravity model
  set Model name = vertical
  subsection Vertical
    set Magnitude = 9.81
  end
end
```

Figure 4: Example of a part of an input parameter file

2.2 Discretization of the domain

The 2D domain of the cross section through the Western Mediterranean has to be divided in smaller areas to compute parameters like pressure, temperature and velocity efficienly at the quadrature points in separate elements. In ASPECT this is done by defining elements, which together form a grid. In this grid, basis functions describe the different variables per element. For this study, Q_2Q_1 elements are used. These elements consist of quadratic basic functions for the velocity variable, and linear basic functions for the pressure variable. A higher order polynomial (e.g. Q_2Q_1 instead of Q_1Q_1) results in a higher accuracy per element, but in an increase of computation time since the amount of degrees of freedom also increases.

2.2.1 Mesh refinement

At the start of each simulation, a uniform global mesh is constructed throughout the whole modelling domain, of which the refinement is determined by the initial global refinement parameter (figure 5a). However, to solve the governing equations in a proper and computationally efficient way, the global mesh needs to be refined at certain places. This refinement can be based on the occurrence of large gradients in temperature or composition, but also on absolute values. In this study, mesh refinement will be based on viscosity gradients, compositional fields and isotherms. To prevent the model from using an extremely large amount of power and memory, the meshes can be refined locally near features of interest, while the global mesh is not refined or even coarsened at locations where no sharp transitions occur. This process of local mesh refinement at the start of the model is called Initial Mesh Refinement (IRS) (figure 5b). Since advection of the material takes place when the model evolves through time, the exact location where large gradients or absolute values are present varies through time. As a result, the mesh needs to be adapted every few time steps. The absolute values of the temperature and the gradients of the viscosity are evaluated again at these time steps. After this, the grid is locally refined or coarsened, depending on the new absolute value and gradient at every location (figure 5c & d). The process of adapting the mesh through time is called Adaptive Mesh Refinement (AMR). It is shown that the use of AMR can significantly decrease the computational time to reach an accurate solution (Kronbichler et al. (2012). Running a model with AMR is a factor 100 faster in 2D, and a factor 1000 in 3D, compared to a model with an equally refined mesh. Using mesh refinement is therefore essential when simulating large domains.

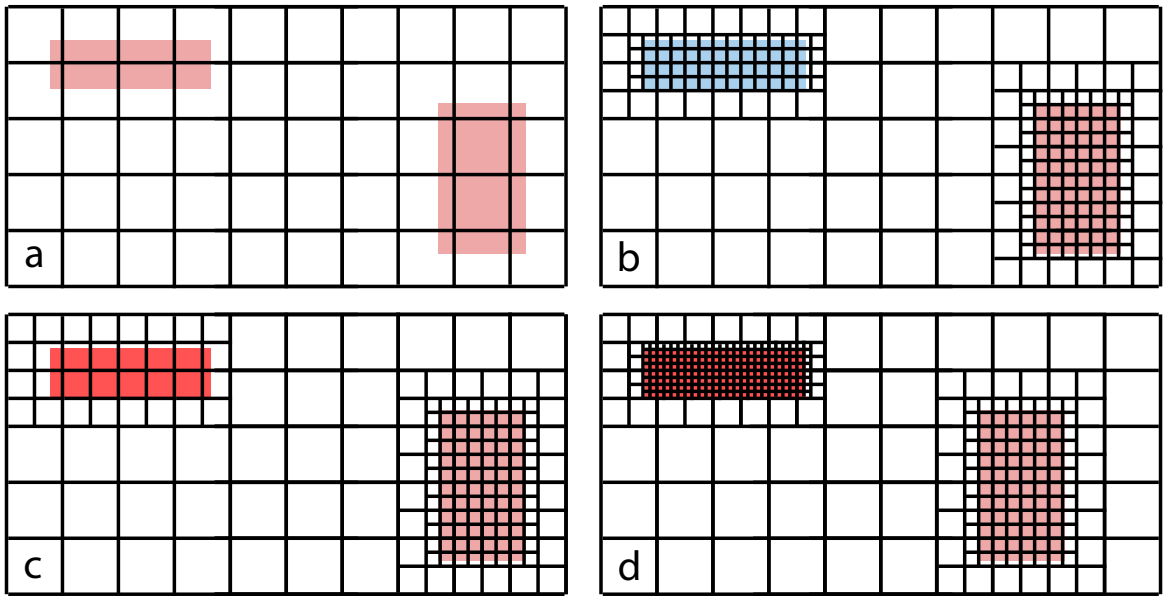

Figure 5: The principle of (adaptive) mesh refinement. In areas with a high gradient/absolute value (red patches) the mesh is refined in the next time step. Areas with a low gradient/absolute value (blue patches) are coarsened. Different levels of refinement can occur (d), depending on the steepness of the gradients/absolute values. Higher gradient (darker red) result in a higher level of refinement

In ASPECT, the user can define the initial global and adaptive mesh refinement, the maximum and maximum level of refinement for elements and the refinement and coarsening fractions. A combination of the values for the initial refinements and the geometry model determines the amount of degrees of freedom for the first time step. For every new level of refinement, a cell is divided into 4 smaller cells. As a consequence, resolution and computation time increase rapidly with increasing refinement level. A maximum/minimum refinement level is needed to prevent infinite refinement/coarsening at locations where gradients remain occurring. The grid setup and refinement has to be chosen properly for the model runs, to ensure a resolution which is high enough to solve the Stokes and temperature equations, but also computationally efficient. The size of the maximum refined cells in this study were approximately 2.5x3.5 km. With this resolution, small scale variations can also be visualized and evaluated.

2.2.2 Time discretization

The choice of the size of the discrete time step is very important in numerical modelling. A time step which is too small will result in an unnecessarily long computation time while a time step which is too big will give an inaccurate solution of the system. To control the size of the time step, ASPECT uses the Courant-Friedrichs-Lewy (CFL) condition. The CFL number is implemented in the calculation of the time step as follows: $dt = CFL * \frac{h_k}{||u||}$, where dt is the time step, h_k is the diameter of a cell K, and $||u||$ is the maximum velocity within cell K. In practice, this means that the time step

is dependent on the size of a cell and on the velocity at which a point moves through that cell, multiplied by a certain factor which is the CFL number. For a CFL smaller than one, a point does not move further than the width of a cell in one time step. For an explicit solving scheme, a CFL-number between zero and one is required to obtain correct results, while an implicit solving scheme can handle values of CFL that are larger than 1. The value of the time step is strongly dependent on the maximum velocity in a cell. A high maximum velocity yields a small time step. When the magnitude of the maximum velocity decreases, the time step could eventually become extremely large. To prevent this to occur, one can define the maximum size of the time step in ASPECT by adjusting the 'maximum time step' global parameter in the input file. For every model run in this study, the maximum time step is chosen to be 1000 years, while the CFL number is set to 0.1.

2.3 Basic equations and variations

Like most geodynamical codes, ASPECT solves a system that describes the motion of a highly viscous fluid, which is driven by differences in gravitational and boundary forces. The difference in gravitational force is caused by variations in the temperature dependent density. This temperature dependent density is given by

$$\rho(T) = \rho_{ref}\Big[1 - \alpha(T - T_{ref})\Big] \tag{1}$$

where α is the linear thermal expansion coefficient and ρ_{ref} is the reference density at reference temperature T_{ref}.

To solve the system, the Stokes equations (2, 3) and the temperature equation (4) are solved. From these equations, velocity $\mathbf{u}$, pressure p and temperature T are obtained:

$$-\nabla\cdot\Big(2\eta\dot{\epsilon}(\mathbf{u}) - \frac{1}{3}(\nabla\cdot\mathbf{u})\mathbf{1}\Big) + \nabla p = \rho(T)g \tag{2}$$

$$\nabla\cdot(\rho\mathbf{u}) = 0 \tag{3}$$

$$\begin{aligned}\rho C_p\Big(\frac{\partial T}{\partial t} + \mathbf{u}\cdot\nabla T\Big) - \nabla\cdot k\nabla T =& \rho H \\ &+ 2\eta\Big(\dot{\epsilon}(\mathbf{u}) - \frac{1}{3}(\nabla\cdot\mathbf{u})\mathbf{1}\Big) : \Big(\dot{\epsilon}(\mathbf{u}) - \frac{1}{3}(\nabla\cdot\mathbf{u})\mathbf{1}\Big) \\ &+ \alpha T(\mathbf{u}\cdot\nabla p)\end{aligned} \tag{4}$$

In these equations, $\dot{\epsilon}(u) = \frac{1}{2}(\nabla u + \nabla u^T)$, which corresponds to the strain rate. The Stokes equation solves the velocity and the pressure field. Both the pressure and velocity vary through the modelling domain through time. The temperature equation is coupled to the Stokes equation in the sense that it depends on the advection with flow velocity $\mathbf{u}$. However, the Stokes equation 2 is also coupled to the temperature equation by the term for the temperature dependent density. The different terms on the right hand side of the temperature equation correspond to the internal heat production due

to radioactive decay, frictional heating and adiabatic heating, respectively. The last two terms can be treated separately in the input file by turning on the shear heating model and adiabatic heating model.

Besides the advection of material through the model domain, there is a fourth basic equation (5) which describes the advection of compositional fields c through the model:

$$\frac{\partial c_i}{\partial t} + \mathbf{u} \cdot \nabla c_i = 0 \tag{5}$$

In ASPECT, a user can divide the modelling domain in several compositional fields. These compositional fields can be used to track a certain composition throughout a simulation, but are also useful in assigning material properties. In these simulations, every distinct material is assigned a different compositional field. Especially in the case of weak zones, this allows tracking of the effect of the material or adjusting one of the material parameters rapidly. Besides the main subdivision in mantle material, overriding plate crust, subducting crust and weak zones, there is also a separate composition for the continental block representing Corsica and Sardinia. This block has the same rheological parameters as the overriding plate crust, but has a higher viscosity due to an adjusted scaling factor ν. The higher value for the scaling factor is implemented to simulate the old, rigid continental block that Corsica and Sardinia consist of. An overview of the different compositions in visible in figure 6a, where every color represents an other compositional field.

2.3.1 Approximate equations

Where the aforementioned equations are used in general to describe the complete system, simplified approximations like the Boussinesq approximation, the extended Boussinesq approximation or the an-elastic approximation are generally used for geodynamical simulations. The use of these equations simplifies the solving of the governing basic equations. The simplification of the equations results in less non-linear dependencies, and therefore less computation time. The physical assumptions made in the approximations are generally slightly inconsistent with the real Earth. However, when the variation between parameters (like density) is small, it is justified to use the approximations to describe the Earth. For example, in the Boussinesq approximation (Boussinesq, 1897) it is assumed that all density variations with respect to a reference state will be neglected, except for the one in the buoyancy term on the right hand side of equation (2). As a result, equation (3) simplifies to

$$\nabla \cdot \mathbf{u} = 0 \tag{6}$$

The visco-plastic material model that is used in this study uses the incompressible formulation of the basic equations. Therefore, (3) is simplified to (6) and the Boussinesq approximation is used. However, in the Boussinesq approximation, both the shear and adiabatic heating terms of equation (4) vanish. The variant where the Boussinesq approximation is used in combination with adiabatic and shear heating is called the extended Boussinesq approximation. In all models performed in this study, the extended Boussinesq approximation with both shear and adiabatic heating is used.

2.4 Extensions to ASPECT

ASPECT does contain a lot of material models and initial setups in its internal code. However, for this study, some custom made or adjusted plugins were needed to prescribe the initial set up of a convergent plate boundary with a subduction interface, especially concerning the initial composition and temperature. All modelling experiments were performed using the Visco Plastic non-linear rheology from the standard ASPECT code, with a minor addition of a factor ν which allows to scale viscosities manually. To assign parameters to the different elements of a subduction zone, several compositional fields were composed. This is done in the *subduction.cc* plugin, which is adjusted from Fraters (2014). The compositions that are assigned in this plugin are passed towards the visco-plastic material model plugin, where it is used to compute the model output parameters.

The second non-standard extension to ASPECT is the plugin for the temperature distribution. For each compositional field, a different initial temperature is described in the *subduction_temp.cc* plugin, which is also adjusted from the plugin from Fraters (2014). The initial temperature set up of the model simulations of this study is dependent on the distribution of the different compositions. The temperature at the top of the model has a constant value of 0 °C, while the mantle temperature increases with a linear geotherm with depth (7).

$$T(z) = T_{pot} + \frac{T_{pot}\alpha g}{C_p}(D_m - z) \tag{7}$$

The overriding plate crust contains a linear geotherm, with a top temperature which equals the surface temperature (0 °C) and a bottom temperature which equals the potential temperature of the mantle on the surface. The subducting plate crust also contains a linear geotherm in the part where the plate is not subducting. The governing equations for the linear geotherms in the overriding plate crust and subducting crust are formulated in equation (8) and (9), respectively.

$$T = T_{top} + \left(\frac{T_{pot} - T_{top}}{h_{OPC}} - \frac{T_{pot}\alpha g}{C_p}\right) \cdot (D_m - z) \tag{8}$$

$$T = T_{top} + \left(\frac{T_{pot} - T_{top}}{h_{SPC}} - \frac{T_{pot}\alpha g}{C_p}\right) \cdot (D_m - z) \tag{9}$$

where h_{OPC} and h_{SPC} are the thicknesses of the overriding plate crust and the subducting plate crust, respectively.

From a certain predefined location onwards, the subducting plate is forced to subduct under the overriding plate, creating a slab. McKenzie (1970) derived an analytical equation which can be solved to obtain an setup of the initial temperature distribution within a sinking slab (10). To formulate this analytical solution, McKenzie (1970) assumed both the top and the bottom of the slab to be in direct contact with mantle material.

$$T(x',z') = \exp\frac{x'\sin\phi - z'\cos\phi}{h'} \cdot \left[T_{pot} + 2(T_{pot}-273)\sum_{i=1}^{\infty}\frac{(-1)^n}{n\pi}\exp\left(R-\sqrt{R^2+n^2\pi^2}\right)x'\sin\left(n\pi z'\right)\right] \tag{10}$$

In this equation $x' = \frac{x}{l}$, $z' = \frac{z}{l}$ are the dimensionless x and z coordinates and h' is the dimensionless scale height, which is given by $h' = \frac{C_p}{\alpha g l}$. The R in the summation term is the thermal Reynolds number, which is calculated using $R = \frac{\rho C_p v l}{2\kappa}$.

To simulate the setting in the Western Mediterranean in a proper way, the implementations of weak zones is needed. A weak zone is an area where the material is locally weakened compared to the surrounding material. Weak zones are not part of the standard code of ASPECT, and therefore it is implemented in the aforementioned plugins for composition and temperature. To implement the weak zones, a separate compositional field is prescribed, which overwrites the earlier assigned composition. The user can manually define parameters like location, weakness and shape of the inherited weak zones.

Both the composition and the temperature extension allow for many customization of the parameters in the input file. The user can set thicknesses, lengths and angles of all different compositions in the modelling domain.

2.5 Solvers

The basic equations of ASPECT of section 2.3 have to be solved during every time step. To achieve this, the basic equations have to be discretized and written into a linear system of equations. The basic form of this system of equations is

$$\boldsymbol{A}\ \boldsymbol{x} = \boldsymbol{b} \tag{11}$$

In this equation, $\boldsymbol{A}$ is a $n \times n$ matrix, $\boldsymbol{x}$ is the vector of n unknowns like temperature and pressure, and $\boldsymbol{b}$, the right hand side of the equation, is the vector of knowns with size n, where n is the number of unknowns in the system.

Solving this system of equations can be done with different types of solvers. However, there are two types of solvers which are primarily used. The first one, the direct solver, is a solver which gives an exact solution by methods that require memory storage of equation 11. Therefore, it is not suitable for solving large realistic or geodynamical problems. The other type of solver is the iterative solver. This type of solver uses a lot less memory and is therefore a better choice for large geodynamical problems. The main differences compared to the direct solver is that an iterative solver requires an initial guess for the vector of unknowns $\boldsymbol{x}$, and tries to converge to the exact solution by an iterative sequence of approximate solutions. After a certain time, the updated solution falls within a user defined norm of the residual of the linear system (the tolerance), and the system is considered solved. The choice of the tolerance is important in solving the system adequately. When the tolerance is set large (e.g. 10^{-2}), the computational time

will be short, but the solution and model output may be not accurate enough. However, when the tolerance is set too small, computational time will increase drastically. Hence, a good trade-off between accuracy and computational time has to be found to solve the system in a efficient way. In my model runs the temperature solver tolerance ($5 \cdot 10^{-12}$) and the linear solver tolerance (10^{-5}) are set to these values. Furthermore, there is a non-linear solver tolerance (10^{-5}). This solver is used for solving the non-linearities in the coupled system, which will be described in the next paragraph.

Besides solving the Stokes equations (2) and (3) and the energy equation (4) separately, it is also possible to solve more complex and coupled systems. In a coupled system, the solution of an equation depends on the solution of an other equation. In the case of the basic equations of ASPECT, it can be seen that the energy equation (4) depends on velocity and pressure, while the Stokes equation (2) depends on temperature.

Solving coupled equations is relatively easy in a linear system. However, the equation for the conservation of momentum (2) is dependent on the viscosity, which is non-linearly dependent on stress and strain rate, and therefore velocity. Solving a linear system is computationally much easier and cheaper than solving a non-linear system. Solving the Stokes and temperature equations requires a lot of computational power. During the model runs of this study, the iterated Stokes non-linear solver scheme is executed. This scheme solves the temperature equation only once at the beginning of each time step. The rheology of the system is non-linearly dependent on this temperature. The solution for the temperature is then used to iterate toward the solution of the Stokes equation (Bangerth et al., 2017). Since the non-linearity of the rheology has a strong influence on the solution of the Stokes equation, these so-called non-linear iterations are needed for every time step, contrary to the solution for the temperature.

2.6 Viscosity averaging schemes

Subduction zone models generally include multiple compositional fields (e.g. crust, upper mantle and lower mantle) with varying parameters in a relatively small domain. For instance, a subducting slab is rheologically stronger than the surrounding mantle material with which it is in direct contact. As a result, large viscosity jumps occur at a small length scale (i.e. 1-10 km), and different compositional fields can be present close to each other. If a certain quadrature point, which is a point used for discrete integration of model quantities, in a cell contains data from multiple compositions, an average of these values has to be found to determine the overall parameter used at that quadrature point. To resolve the problem of having multiple compositions and viscosities at a quadrature point, different viscosity averaging schemes can be implemented. In these averaging schemes, the compositional values are evaluated at every quadrature point and replaced by a new average value depending on the chosen averaging scheme. For a harmonic averaging scheme, the original value is replaced by the harmonic average, which is calculated using $\vec{x} = \left(\frac{1}{N}\sum_{i=1}^{N}\frac{1}{x_i}\right)^{-1}$. Here, N is the amount of values which is evaluated for each averaging calculation. For a geometric averaging scheme the

averaged value becomes $\vec{x} = \left(\prod_{i=1}^{N} \frac{1}{x_i} \right)^{\frac{-1}{N}}$. The main difference between the harmonic and geometric average is that the sum of the reciprocal parameters is used for the harmonic average, while for the geometric average the n^{th} root of the products of n parameters is used. Both the geometric and harmonic average are (together with the arithmetic mean) part of the Pythagorean means. Of these means, the harmonic mean always gives the lowest resulting mean when the separate evaluated values are positive. Hence, if the averaging schemes are applied to the viscosity computed at a quadrature point, the lowest viscosity is dominant for the harmonic average. For the geometric average, the calculated mean value will always be higher than the harmonic average if the same values are used to calculate the mean. In the result section of this study, both models with a harmonic and geometric mean will be discussed. It is noted that the harmonic averaging scheme has a physical basis of assuming the various deformation mechanisms to operate under the same stress (Berg et al., 1993).

3 Subduction modelling and boundary conditions

3.1 Model setup

The 2D-model which is used to simulate the geological setting of the Western Mediterranean has a box geometry with a width of 2400 km and a thickness of 760 km, and is confined to the upper mantle (660 km) plus a small layer of lower mantle material (100 km). Figure 6a shows the general set up for all simulations in this study. The domain comprises mostly of mantle material, which is overlain by a continental overriding plate crust at the right part of the domain, and a subducting oceanic crust on the left. A continental block representing Corsica-Sardinia is implemented, and has a width of 250 km. The strip of lower mantle material is implemented in the bottom of the model, to assure a correct simulation when open vertical boundaries are implemented and free slip is imposed on the bottom boundary. Every colour represents a different compositional field. The rheological parameters of the two weak zones can be adjusted independent.

The location of subduction onset in the model is prescribed in the input parameters file, and can be adjusted manually by the user. To assure that the pressure profile on both vertical boundaries during a run with open boundaries is the same, a small strip of oceanic lithosphere is placed on the utter right of the box. Weak zones are implemented to represent initial weaknesses in the overriding plate, caused by the presence of sutures and/or plate boundaries as described in section 1.1. In the following section, an explanation will be given on the choices made regarding the velocity and rheological boundary conditions.

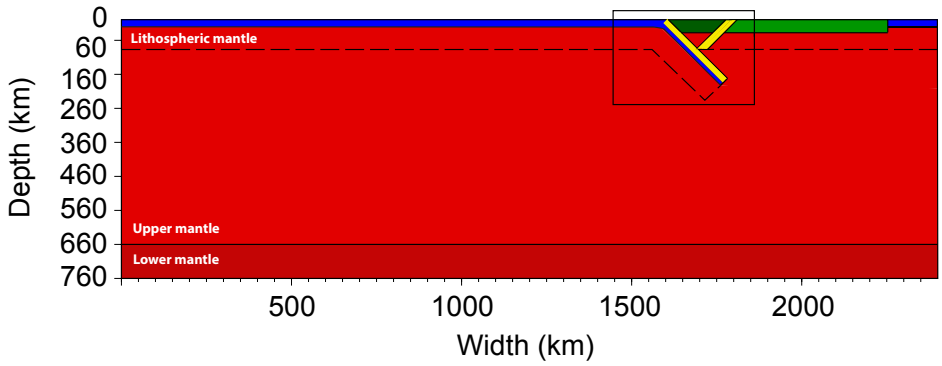

(a)

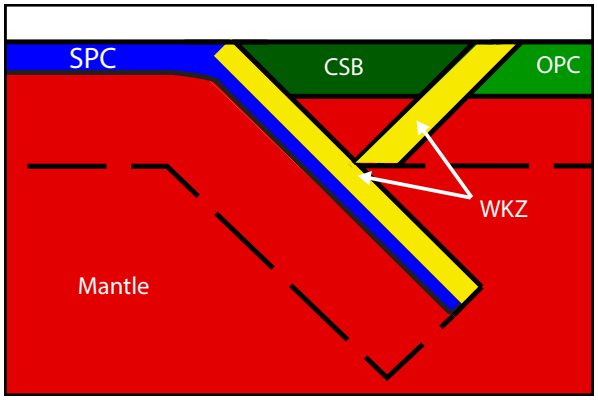

(b)

Figure 6: a) Setup of the model where each color corresponds to an other composition. The dashed line indicates the boundary between the lithospheric and asthenospheric mantle; b) Zoom-in on the area where the subduction zone is implemented. WKZ = Weak Zone, SPC = Subducting plate crust OPC = Overriding plate crust, CSB = Corsica-Sardinia Block

3.2 Velocity boundary conditions

The four boundaries of the model each have other boundary conditions regarding the velocity, which also vary through time depending on the evolution of the model. The top boundary is the same for each model and represents the Earth's surface. Since free slip or no slip is not a realistic representation of the Earth's surface, a free surface is used for this boundary (Rose et al., 2017). This allows the material to freely flow according to the solution of the Stokes equations in both a vertical and horizontal direction, causing topography and back-arc basins to form in a realistic way. Since flow through the original boundary of the model is possible, a dynamically deformable mesh is required to satisfy the conservation of mass in the modelling domain. To handle the vertical motions in a correct way, ASPECT uses an Arbitrary Lagrangian-Eulerian framework. This framework tries to combine the benefits of both the Lagrangian (mesh moves with fluids, but quick distortion) and Eulerian (fixed meshes that do not move with fluid motions) meshes.

The use of a free surface can cause small disequilibria in the location of the free surface. Hence, the free surface needs to be stabilized to prevent the free surface advection from overshooting. This stabilization (Kaus et al., 2010) can be done by setting a stabilization parameter θ at a value between 0 (no stabilization) and 1 (full stabilization). In the models carried out in this study, θ is set to 1.

Whereas the bottom boundary of the model has a fixed no slip boundary condition, the vertical left and right boundaries of the model have varying boundary conditions. During the first stages of the model, the boundary conditions regarding velocity will be prescribed, while they are set to open boundaries at a certain point in most of the model runs. Hence, both prescribed boundary velocities and open boundaries are used, which I will elaborate on in the coming section.

3.2.1 Prescribed velocities

Material in- and outflow along the vertical boundaries is controlled by the amount of inflow resulting from the convergence velocity of the two plates. The prescribed boundary velocities in this study are a projection of the absolute plate motions between Africa and Europe on the 2D cross section. It is assumed that the absolute plate motion of Africa with respect to Europe is perpendicular to the 2D cross section on the western (right) boundary, while there is a small velocity component in the plane of the cross section on the eastern (left) boundary. In practice, this means that the inflow velocity of subducting plate material is set to 0.5 cm/y for most of the models, while the overriding plate is kept fixed. Deviations in plate velocity boundary conditions will be discussed in the results section.

The velocity boundary conditions for the vertical boundaries of the model are defined using the principle of conservation of mass in the system. The total amount of inflow of material in the model is equal to the total amount of outflow. Assuming a constant inflow velocity of material of the subducting slab, a mass balance can be composed. The volume of material flowing in the box is equal to the thickness of the subducting slab (H_{sl}) times the incoming velocity of the subducting plate ($V_{I,L}$). At a large depth in the model, the influence of drag from the material flowing in at the top of the model is negligible, resulting in a dominance of outflow of material. This outflow can be calculated by multiplying the outflow velocity ($V_{O,L}$) by the total area of this zone, which is $D_m - H_{sl} - H_z$, with D_m being the total depth of the model, and H_z the thickness of the transition zone between the subducting plate and the point were the influence of the drag due to inflow becomes negligible. The transition zone is introduced to account for the change from a net inflow to a net outflow of material. The velocity profile in this zone is treated as a linear function, with a dependence of the outflow velocity on the inflow velocity. The derivation of the outflow velocity is as follows:

$$H_{sl}|V_{I,L}|+\frac{1}{2}\frac{H_z\cdot|V_{I,L}|}{|V_{I,L}|+|V_{O,L}|}|V_{I,L}|=\frac{1}{2}(H_z-\frac{H_z\cdot|V_{I,L}|}{|V_{I,L}|+|V_{O,L}|})|V_{O,L}|+(D_m-H_{sl}-H_z)|V_{O,L}|$$

$$H_{sl}|V_{I,L}|+\frac{1}{2}\frac{H_z\cdot|V_{I,L}|}{|V_{I,L}|+|V_{O,L}|}|V_{I,L}|=-\frac{1}{2}\frac{H_z\cdot|V_{I,L}|}{|V_{I,L}|+|V_{O,L}|})|V_{O,L}|+(D_m-H_{sl}-\frac{1}{2}H_z)|V_O|$$

$$H_{sl}|V_{I,L}|+\frac{1}{2}\frac{H_z\cdot|V_{I,L}|}{|V_{I,L}|+|V_{O,L}|}(|V_{I,L}|+|V_{O,L}|)=(D_m-H_{sl}-\frac{1}{2}H_z)|V_{O,L}|$$

$$H_{sl}|V_{I,L}|+\frac{1}{2}\frac{|V_{I,L}|+|V_{O,L}|}{|V_{I,L}|+|V_{O,L}|}(H_z\cdot|V_I|)=(D_m-H_{sl}-\frac{1}{2}H_z)|V_{O,L}|$$

$$H_{sl}|V_{I,L}|+\frac{1}{2}H_z\cdot|V_{I,L}|=(D_m-H_{sl}-\frac{1}{2}H_z)|V_{O,L}|$$

$$|V_{O,L}|=\frac{(H_{sl}+\frac{1}{2}H_z)|V_{I,L}|}{D_m-H_{sl}-\frac{1}{2}H_z}$$

The resulting $|V_{O,L}|$ is the magnitude of the outflow velocity in the mantle on the left boundary of the model, below the transition zone, assuming no mantle wind. On the left boundary, the direction of the flow is taken in the negative x-direction.

The derivation of the flow velocities on the right boundary is similar to that for the left boundary. Assuming mass conservation in the model, the velocity boundary conditions of the model become:

1. $V_{I,L}$ for $x=0$ & $D_m-H_{sl}<z<D_m$
2. $V_{I,L}-\frac{V_{I,L}+V_{O,L}}{H_z}*(D_m-H_{sl}-z)$ for $x=0$ & $D_m-H_{sl}-H_z<z<D_m-H_{sl}$
3. $-V_{O,L}$ for $x=0$ & $z<D_m-H_{sl}-H_z$
4. $V_{I,R}$ for $x=modellength$ & $D_m-H_{op}<z<D_m$
5. $V_{I,R}-\frac{V_{I,R}+V_{O,R}}{H_z}*(D_m-H_{op}-z)$ for $x=modellength$ & $D_m-H_{op}-H_z<z<D_m-H_{op}$
6. $-V_{O,R}$ for $x=modellength$ & $z<D_m-H_{op}-H_z$

In these cases, $V_{O,L}=\frac{(H_{sl}+\frac{1}{2}H_z)|V_{I,L}|}{D_m-H_{sl}-\frac{1}{2}H_z}$ and $V_{O,R}=\frac{(H_{op}+\frac{1}{2}H_z)|V_{I,R}|}{D_m-H_{op}-\frac{1}{2}H_z}$ For the model runs in this study, $|V_{I,R}|$ is 0, since the overriding plate is kept fixed. As a result, there is no mantle outflow resulting from incoming plate material. Figure 7 indicates the direction and relative magnitude of flow, corresponding to the places where this flow occurs.

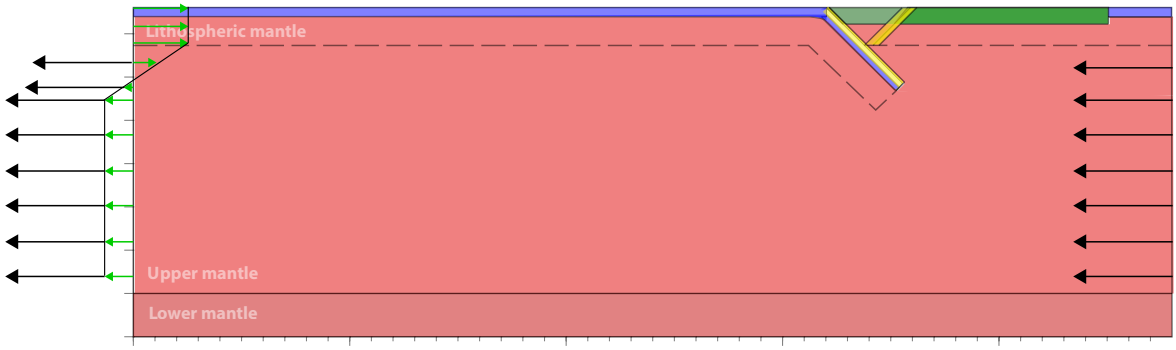

Figure 7: The velocity boundary conditions for each model set up. The overriding plate is kept fixed, while there is a small convergence velocity of the subducting plate (green arrows). There is an equilibrium in inflow and outflow of material. The black arrows indicate the mantle wind.

Besides the prescribed in- and outflow velocities due to the plate motions, an extra velocity component can be used in the mantle. While the outflow of material previously was needed to satisfy the conservation of mass, now it is introduced to simulate the toroidal flow which normally takes place around the slab edges in 3D Dvorkin et al. (1993). However, since we are modelling in 2D, this toroidal flow can not be incorporated in the model. To overcome this problem, an outflow of mantle material at the left boundary is introduced to simulate the disappearing mantle material behind the slab. The amount of mantle material that flows out of the model at the left boundary, is equal to the estimated amount of material in the toroidal flow. The amount of toroidal flow is estimated by multiplying the depth difference between the original location of the slab tip and its final depth (the 660), and the amount of rollback during the model run. The calculated volume will then be distributed over the whole mantle domain, and the amount of outflow of material will be time independent. The outflow on the left is compensated at the right boundary with an inflow of the same volume of material to satisfy the conservation of mass of the system. The mantle wind is set at 1.8 cm/yr for every model in this study.

3.2.2 Open boundaries

When the slab tip has reached the 660 km discontinuity, the model domain is effectively being divided into two separated compartments as escape flow underneath the slab tip is impossible. The earlier described forced mantle wind will be switched off and the dynamics of the system will be solely responsible for all motions. From this point onwards, the vertical boundaries will act as open boundaries. To prevent a drain of the domain, the normal component of traction on the vertical boundaries has to be prescribed. In my models, the lithospheric pressure along the boundaries is calculated using the initial lithostatic traction model from the ASPECT internal code or using time and position dependent plugin provided by Anne Glerum (personal

communication). The plugin by Anne Glerum calculates the governing pressure at every time step (contrary to the initial lithostathic traction model), and is based on the current temperature and composition distribution. Using the "Box with lithosphere boundary indicators" geometry model, the boundary conditions in the lithosphere (convergence velocity) can still be adjusted.

3.3 Rheological parameters

All models in this study use the visco-plastic material model from the standard library of ASPECT. The visco-plastic material model takes into account both brittle (plastic) and non-linear viscous deformation. This allows ASPECT to model complex lithospheric processes. The dominant deformation mechanism is determined by the amount of stress and the temperature. While plastic (permanent brittle) deformation is the dominant deformation mechanism in the crustal part of the lithosphere, non-linear viscous deformation becomes increasingly important at larger depth and in the mantle. Figure 8 shows the different deformation mechanisms as a function of temperature and pressure.

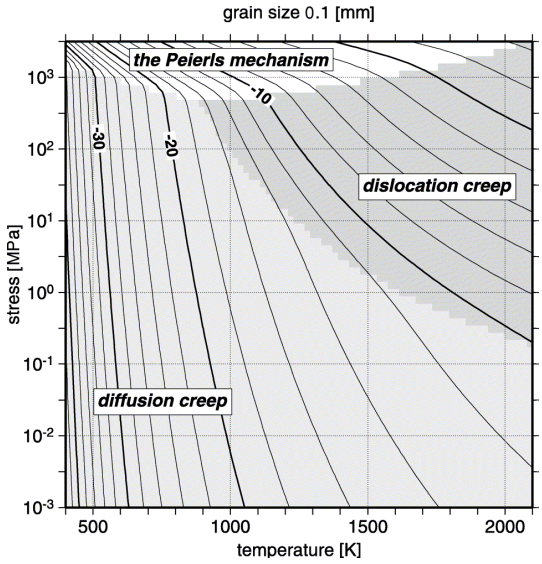

Figure 8: Deformation map of the governing deformation mechanism as a function of stress and temperature for a grain size of 0.1 mm. The solid lines indicate a constant strain rate, while the colored areas indicate the dominant deformation mechanism. Figure from Kameyama et al. (1999)

The material model is used to calculate the viscosity throughout the whole model domain, and its evolution through time. At every time step, the viscosity for dislocation creep and diffusion creep is calculated for every quadrature point by the following equation:

$$\mu = \frac{1}{2}\nu A^{-\frac{1}{n}} d^{\frac{m}{n}} \dot{\epsilon}_{ii}^{\frac{1-n}{n}} exp\Big(\frac{E+PV}{nRT}\Big) \tag{12}$$

where ν is a factor to control weakening or hardening manually, A is the prefactor, n is the stress exponent, $\dot{\epsilon_{ii}}$ is the square root of the deviatoric strain rate tensor second invariant, d is grain size, m is the grain size exponent, E is the activation energy (the energy that must be overcome to let a reaction occur), V is the activation volume for this reaction, P is pressure, R is the gas exponent and T is the temperature.

In ASPECT, the user can define the governing viscous flow law. A choice can be made between diffusion creep, dislocation creep and composite, where the composite flow law comprises both diffusion creep and dislocation creep through the following relation:

$$\mu_{eff} = \frac{\mu_{disl} \cdot \mu_{diff}}{\mu_{disl} + \mu_{diff}}$$

Using the composite flow law, one can account for a broader range of viscosities in one model run. When a composite viscosity formulation is used, the effective viscosity is lower for a higher strain rate, enhancing localization of deformation (Morra, 2015). However, viscous deformation is not the dominant deformation mechanism in the whole domain. Viscosity is limited by a plastic yielding mechanism. In this study, a Drucker Prager Yield Criterion is used, which in 2D is equal to the Mohr Coulomb Criterion:

$$\sigma_y = C \cos\phi + P \sin\phi$$

In this equation, C is the cohesion of the material, and ϕ is the angle of internal friction. When the viscous stress, which can is calculated by $2\mu\epsilon_{ii}$ is larger than the yield stress σ_y, plastic deformation is the main deformation mechanism and the material deforms in a brittle way. In this case, the viscosity re-scaled to the yield surface using $\mu_y = \frac{\sigma_y}{2\mu\epsilon_{ii}}$, and this viscosity is assigned to the quadrature point.

Most of the rheological parameters used in the model are determined empirically in laboratory experiments. While it is possible to perform the laboratory experiments at upper mantle temperatures, simulation of the stress is much harder. Extrapolation of the laboratory data to mimic geological conditions is required, and results in a lower accuracy of the rheological constraints (Hirth and Kohlstedt, 2003). As a consequence, a broad range of possible values for the different parameters in equation (12) is available from different laboratory experiments (Karato and Wu, 1993; Gleason and Tullis, 1995; Hirth and Kohlstedt, 1996, 2003). The rheology of a material is highly sensitive to small changes in parameters. This complicates the choice of a good combination of values. Table 1 shows the rheological parameters which are used for the main compositions in the modelling experiments of this study. The mantle material in the model is represented by wet olivine. For dislocation creep in wet olivine, the parameters for the stress exponent, the activation energies and volumes and the stress exponent are derived from Karato and Wu (1993). For diffusion creep, the parameters from Hirth and Kohlstedt (2003) are implemented. The parameters for dislocation creep in the overriding plate crust (OP crust) are derived from Gleason and Tullis (1995), which are obtained from laboratory measurements on quartzite.

For dislocation creep, the viscosity does depend non-linearly ($n \neq 1$) on the strain rate, while there is no grain size dependency ($m = 0$). However, for diffusion creep, there is a linear dependence on strain rate ($n = 1$), but it depends non linearly on the grain size ($m = 3$) (Hirth and Kohlstedt, 2003) (see also table 1).

Parameter	**U. mantle**	**L. mantle**	**Subd. crust**	**OP crust**
Density ($kg \cdot m^{-3}$)	3300	3300	2900	2700
Angle of internal friction (°)	30	30	30	30
Cohesion (MPa)	20	20	20	20
Disl. activation energy ($kJ \cdot mol^{-1}$)	4.8e5	4.8e5	0	2.23e5
Disl. activation volume ($m^3 \cdot mol^{-1}$)	11e-6	11e-6	0	0
Disl. prefactor ($Pa^{-n} \cdot s^{-1}$)	3.9063e-15	3.9063e-15	1e-21	1.1e-28
Disl. stress exponent	3	3	1	4
Diff. activation energy ($kJ \cdot mol^{-1}$)	335e3	335e3	335e3	335e3
Diff. activation volume ($m^3 \cdot mol^{-1}$)	4.0e-6	4.0e-6	4.0e-6	4.0e-6
Diff. prefactor ($Pa^{-n} \cdot s^{-1}$)	1.92e-20	1.92e-20	1.92e-20	1.92e-20
Diff. grain size exponent	3	3	3	3
Reference temperature (K)	273.15			
Reference viscosity ($Pa \cdot s$)	$1.0 \cdot 10^{21}$			

Table 1: Rheological parameters for the different main compositional fields

The parameters for the continental block and the weak zones are similar to the parameters of the overriding plate crust and the composition the weak zone is inherited, respectively. For both the continental block and the weak zones, only the scaling factor ν is adjusted compared to the original composition.

4 Results

During the process of simulating the geological setting of the Western Mediterranean in a 2D model, adjustments on the initial set up have been made to run different models. The set ups have been used in models with both a geometric and an harmonic averaging scheme. The results of these performed model runs will be elaborated on separately in this section.

4.1 Harmonic averaging scheme

The first tests include the tests with an harmonic averaging scheme. This averaging scheme is the most natural way of implementing a compositional averaging scheme (see section 2.6). Different tests have been performed, where every test has different boundary velocity conditions or a different strength of the overriding plate.

4.1.1 Prescribed velocities

The first models are models with prescribed velocities on the vertical boundaries during the whole model run. In this section, the evolution of two of those models will be evaluated. They have the same set up, except for the prescribed velocity boundary conditions. The inflow velocity of subducting plate material is 0.5 cm/yr for both models, and the outflow velocity on the vertical boundaries is dependent on the inflow velocity only for the first model. For the second model, the outflow velocity is dependent on the inflow velocity, but the enhancing mantle wind to simulate the toroidal flow around the slab edges is also implemented. The amount of mantle wind is 1.8 cm/yr, calculated as described in section 3.2.1 Both models have an inherited weak zone in the overriding plate between the Corsica-Sardinia block and the overriding plate representing the European mainland. The material in the weak zone is 10000x weaker than the material in the surrounding overriding plate. Without a weak zone in the overriding plate, localization of deformation is not present and rollback does not take place. Furthermore, the dip of the slab is set to 60 °, instead of the usual 45 °from the general model setup.

Model without mantle wind Figure 9a shows the temporal evolution of the model without mantle wind. During the first 15 million years, vertical sinking of the slab and rollback of the trench is present. There is a localization of deformation in the inherited weak zone, were the viscosity remains low due to a high strain rate. Extension focuses here, causing the rollback of the slab to continue. When the slab tip approaches the 660 km discontinuity it flattens horizontally, which indicates that stagnation of the slab at the 660 is absent. The velocity vectors show the governing velocity field. The horizontal flow at the bottom of figure 9a plays a major role in the development of the model, primarily between 12.5 My and 15 My. The presence of this horizontal flow is mainly controlled by the choice of the boundary conditions on the vertical boundaries. The rollback of the slab causes the pressure in the compartment behind the slab to increase, since the outflow on the vertical boundaries is prescribed and independent of pressure. Furthermore, material is not able to go through the bottom boundary due to the free slip condition. As a result the compartment behind the slab gets over-pressured, and the only possibility for the mantle material is to escape underneath the slab to the low-pressure area in the extensional domain of the model. The slab is flattened and does not reach the 660 discontinuity, which should be the case according to tomographic images (figure 3). The total amount of rollback in the first 15 million years is approximately 200 km, which is only a part of the total amount of extension of the Liguro Provençal basin. Furthermore, no stagnation occurs when the slab reaches the 660 since the slab is not approaching it vertically, indicating that this set up does not validate the Faccenna et al. (2001) hypothesis.

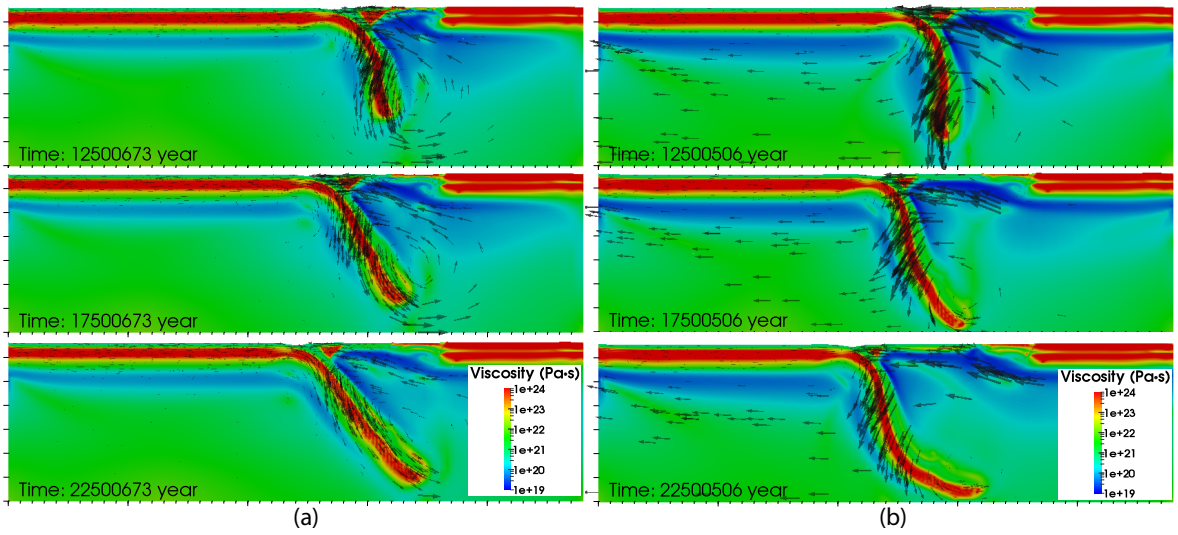

Figure 9: a) Evolution of a model without mantle flow. The black arrows represent the velocity vectors in the modelling domain. The large component of horizontal flow beneath the slab is primarily visible in figure between 12.5 and 15 My, resulting in a flattening of the slab; b) Model with mantle flow. Slab dips steeper, and no escape flow occurs. Slab is draped along the 660. Note: no lower mantle incorporated in these models.

Model with mantle wind The evolution of the model of figure 9a, but with a mantle wind, is visible in figure 9b. The evolution in the first million years is relatively similar to the one without mantle flow, except for the increased steepness and the higher amount of rollback of the slab tip. Due to the continuous push and suction of the mantle material, the dip angle of the slab becomes larger compared to the model without mantle flow. The total amount of rollback after 15 million years of model run is around 300 km, which is 100 km more than in the model without prescribed mantle flow, while all other parameters are the same. The slab tip reaches the 660 km discontinuity, since there is no escape flow due to the continuous suction from the left boundary. However, no stagnation of rollback occurs and the slab is just draped along the 660.

4.1.2 Open boundaries

The implementation of open boundaries solves the problem of the over-pressuring of the compartment below the slab of figure 9a, since material can freely flow in and out of the modelling domain on the vertical boundaries. Only the velocity in the lithosphere of the subducting plate is prescribed at 0.5 cm/yr, all other velocities are a direct result of the dynamics of the system. The model setup is similar to that of the model in section 4.1.1, except for the small strip of oceanic crust at the utter right of the domain to ensure a correct traction at the vertical boundaries and the lower mantle at the bottom. The traction is calculated by the initial lithostatic pressure traction model.

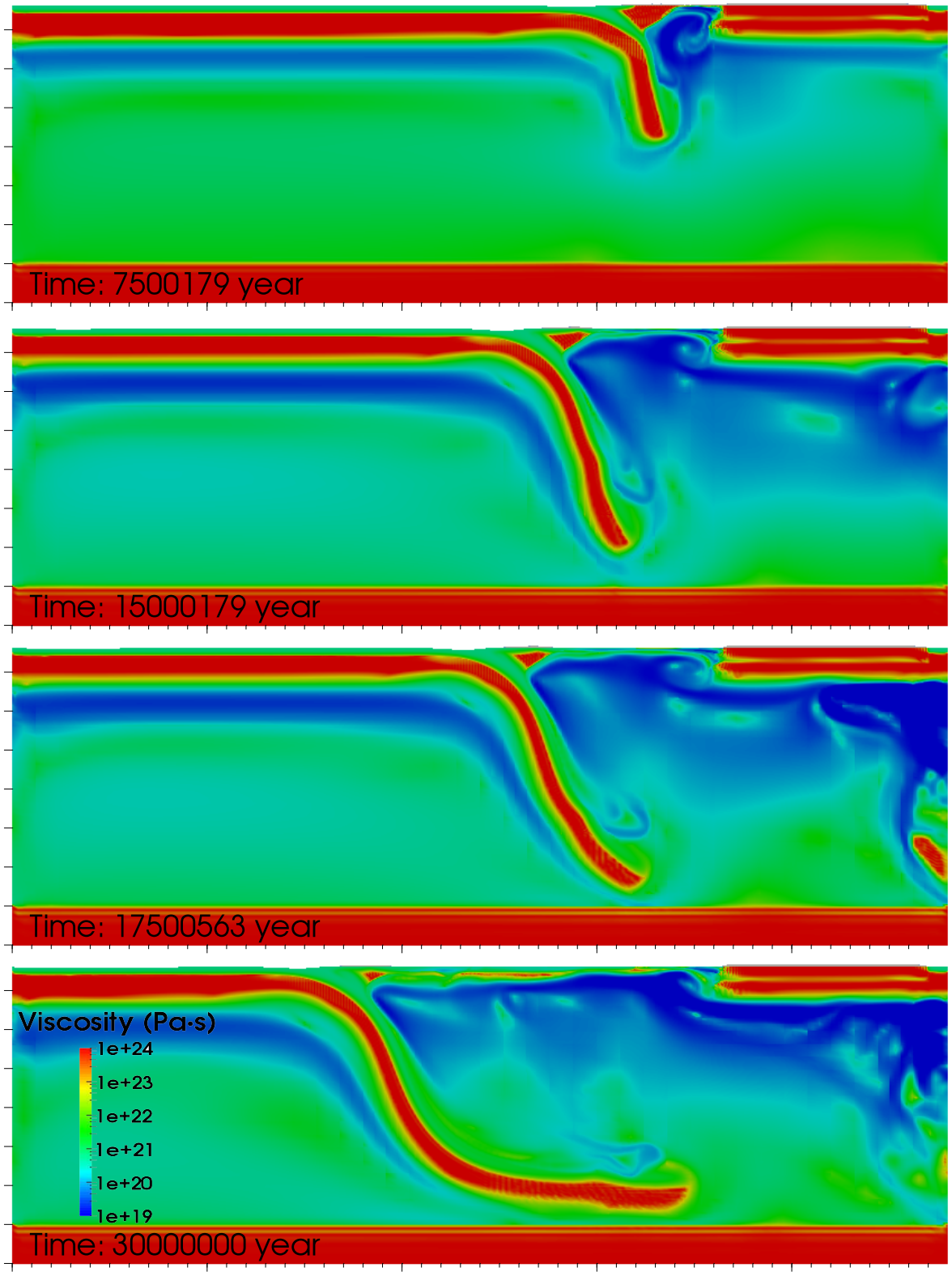

Figure 10: Evolution of a model with an harmonic averaging scheme and open boundaries from the start.

Deformation again focuses in the inherited weak zone during the first stages of the model run. Suction between the slab and the Corsica-Sardinia block causes the block to drift together with the slab. The viscosities in the weaker zone remain low, due to a high strain rate in that area. The zone with a low viscosity gets wider when the model evolves, indicating an ongoing spreading and rollback. The chaotic pattern close to the right boundary of the domain developing from 15 million years onwards is caused by the choice of the boundary traction model. The used traction model for this run only calculated the pressure profile at the beginning of the simulation, and variations in this pressure cause the calculated profile to become inaccurate at a certain point in time.

For both the model with and without mantle wind, the high viscosity Corsica-Sardinia block vanishes through time, and even seems to disappear almost entirely after 30 million years. The disappearing of the rigid block is caused by the choice of the averaging scheme. As mentioned in section 2.6, the harmonic viscosity averaging scheme 'favours' a lower viscosity above a high viscosity when calculating the average viscosity. As a result, the high viscosity is diffused away through time suggesting that the Corsica Sardinia block dissolves through time. However, if the composition of the initial high-viscosity block is tracked through the domain (figure 11), it can be seen that from the original 38 km of crust, 25 km is still left after 30 million years. The block of 25 km has experienced 790 km of rollback in 30 million year, and did not vanish completely, contrary to the expectations if you only look at the viscosities.

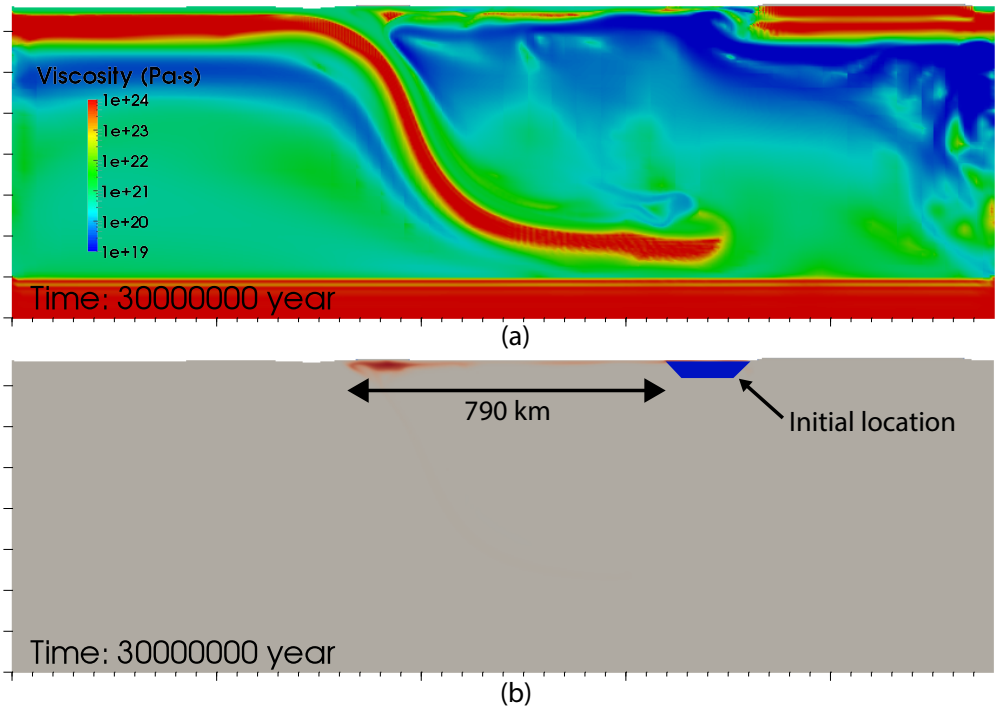

Figure 11: a) Snapshot of the final state of the model from figure 10 as a reference for figure b. b) Distribution of the original distribution of the continental block composition after 30 million years. Distance between initial and final state is 790 km.

4.1.3 Hybrid model

Both the model with the prescribed velocities and the open boundaries are models that do not completely mimic the perceived situation in the Western Mediterranean. The model with prescribed velocities is able to simulate the toroidal flow through a mantle wind. However, when the compartments get sealed, the mantle wind has to be minimized to avoid a forced rollback. On the other hand, using open boundaries is a good way to evaluate the effect on the evolution of the slab dynamics itself, but the toroidal flow around the slab edges can not be simulated. When the boundary conditions of the prescribed velocities and the open boundaries are combined, it is possible to implement a mantle wind during the first stages of the model and use open boundaries from the point the slab has reached the 660 onwards.

The hybrid model has a weak zone between the Corsica-Sardinia block and the overriding plate like the previous models, but it also has an extra weak zone between the subducting plate crust and the Corsica-Sardinia block to facilitate the extension between the retreating slab and the Corsica-Sardinia block at the onset of the reactivation of rollback. This weak zone is 100x weaker than the subducting plate crust itself, and represents the zone with former active faults between Calabria and the Corsica-Sardinia block.

The evolution of the hybrid model is different from the models with prescribed velocities and open boundaries, due to the presence of the second weak zone (figure 12). Instead of having localization of deformation in one of the two weak zones, there is a simultaneous extension in both weak zones from the onset of rollback. This is inconsistent with the geological situation in the region, where the Corsica-Sardinia block remained attached to the retreating slab before the stagnation. The total amount of rollback is also larger than that in the model with the open boundaries. Furthermore, there again is no stagnation of the rollback, despite the enhancing mantle wind.

When the strength of the weak zone between the subducting plate and the Corsica Sardinia block is varied, the evolution of rollback changes significantly (figure 13). The weaker the material in the weak zone, the larger the amount of rollback. If the strength of the material in the weak zone is increased compared to the model where it was 100x weaker, the slab is not detached from the Corsica-Sardinia block and the rollback distribution has changed significantly. A higher initial weakness still causes a lower viscosity in the extensional domain after 15 million years due to a higher strain rate. For the model with the strongest weak zone (only 2 times weaker than the original slab crust), there is still no detachment around 15 million years which is more realistic than the simultaneous extension. However, flattening of the slab occurs in every case, and there is still no stagnation and reactivation of rollback.

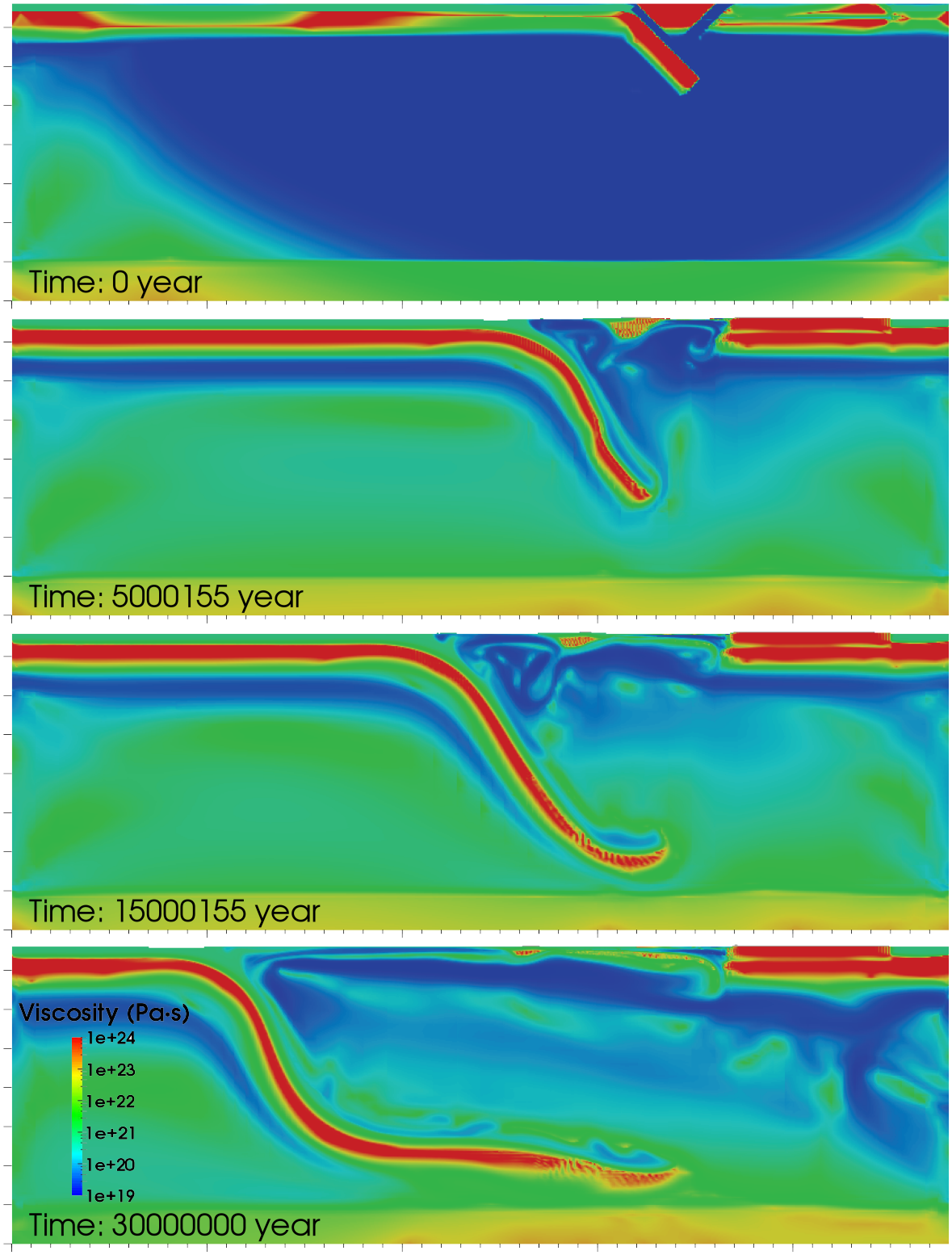

Figure 12: Evolution of a model with hybrid velocity boundary conditions and two weak zones. Open boundaries are implemented after 18 million years. Simultaneously spreading in both weak zones

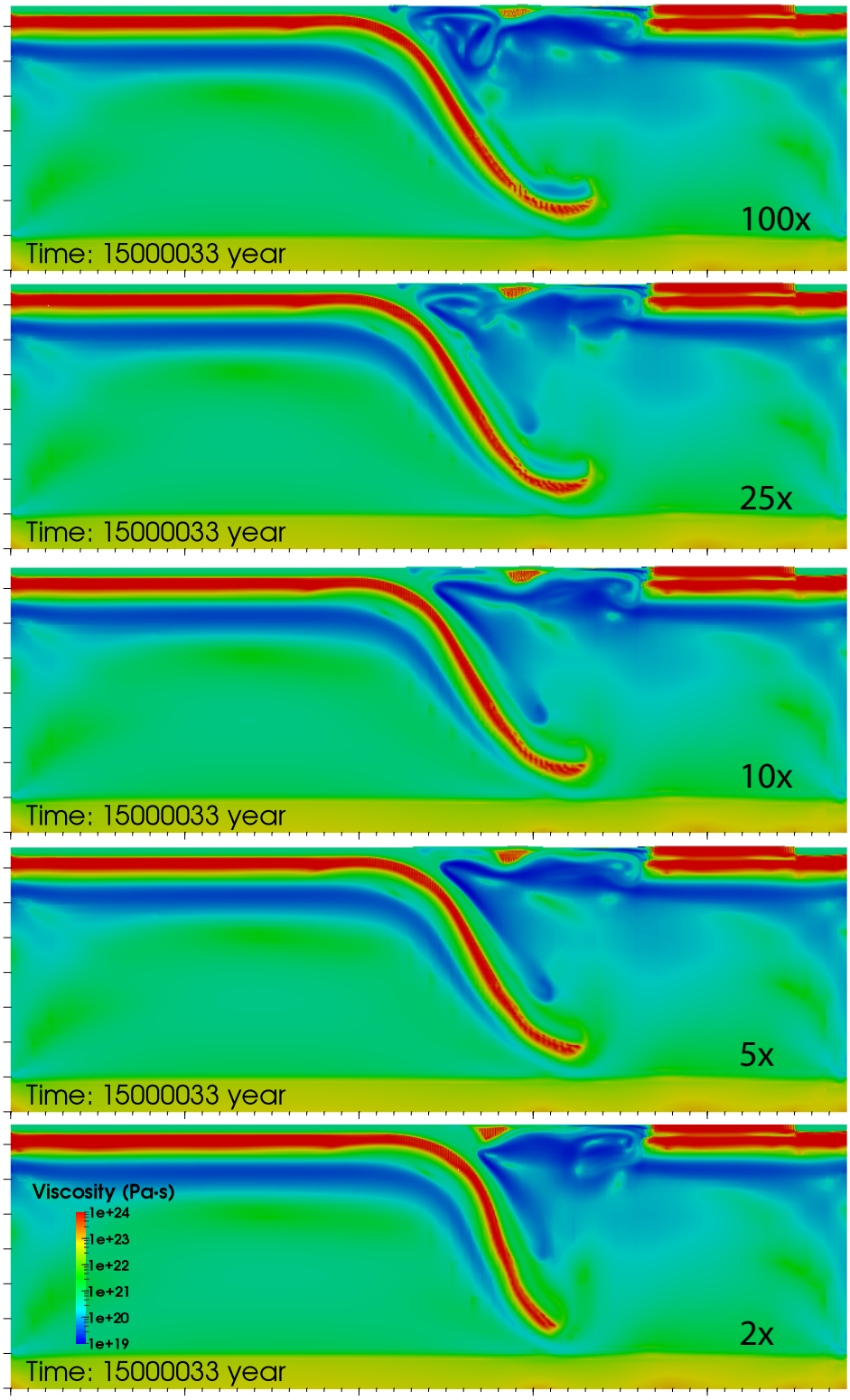

Figure 13: Snapshot after 15 million years of models with different strength of the weak zone. Weakening factor compared to subducting plate crust material is indicated in the bottom right. The first snapshot corresponds to the model of figure 12

4.2 Geometric averaging scheme

The geometric averaging scheme, which gives a higher average viscosity when the compositions at a quadrature point are averaged (see section 2.6), is implemented in the following models. A higher viscosity indicates a more rigid block, and may play an important role in the detachment from the subducting plate.

4.2.1 The effect of weak zones

As discussed in section 1.1, the implementation of a weaker zone in the overriding plate is necessary to simulate the presence of a suture or fold and thrust belt on the plate boundary between the Corsica-Sardinia block and the European mainland. The properties of this weak zone are described in the rheological parameter section. Both the weak zones between the slab and the Corsica-Sardinia block and the overriding plate and the Corsica-Sardinia block are removed, resulting in one rigid overriding plate. In this case, rollback of the slab is not initiated and the subduction system is locked (figure 14). This is the case for both the model with (figure 14a & b) and the model without (figure 14c & d) initially prescribed mantle wind. The main difference between those two models is that the slab is more curved throughout the model run, which is primarily visible in figure 14c. After the mantle flow is turned off after 14.5 million years, the weight of the slab causes it to move back to a equilibrium position, where it sinks more vertically. However, after 30 million years you can still see the effect of the mantle flow in the first stages of the simulation, since the slab sinks more vertically than in the case where no mantle wind was present. The viscosity of the crustal material of the slab in the subduction channel is relatively high, causing the locking of the system. The material around the slab itself has a somewhat lower velocity due to a high strain rate. There is no rollback of the slab for this simulation.

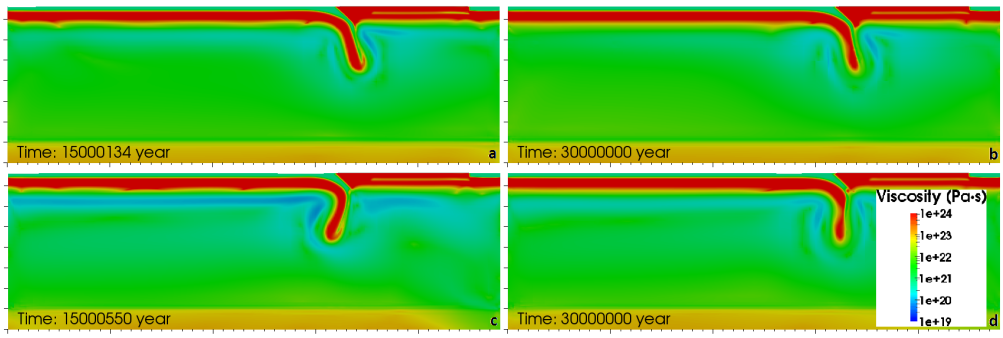

Figure 14: Model run without weak zones between the Corsica-Sardinia block and the rest of the overriding plate. a) Model without prescribed mantle flow after 15 My; b) Final state of the model without prescribed mantle flow after 30 My; c) Model with prescribed mantle flow after 15 My; d) Final state of the model with prescribed mantle flow after 30 My

4.2.2 Prescribed velocities

The model with prescribed velocities and a geometric average (figure 15) uses the same model set up as that of the harmonic average with mantle flow (figure 9b). The main difference in model evolution is that the subduction system is locked, and that there is no rollback of the slab at all. The curvature of the slab after 15 and 30 million years is caused by the constant mantle wind through the domain. Rollback is not initiated, like in the model without weak zones, because the localization of deformation does not cause the strain rate to increase and the viscosity to decrease enough in the inherited weak zone. As a result, hot material is not able to flow in the weak zone anymore, preventing rollback to start. The overall viscosity in the domain is also lower than for the harmonic average.

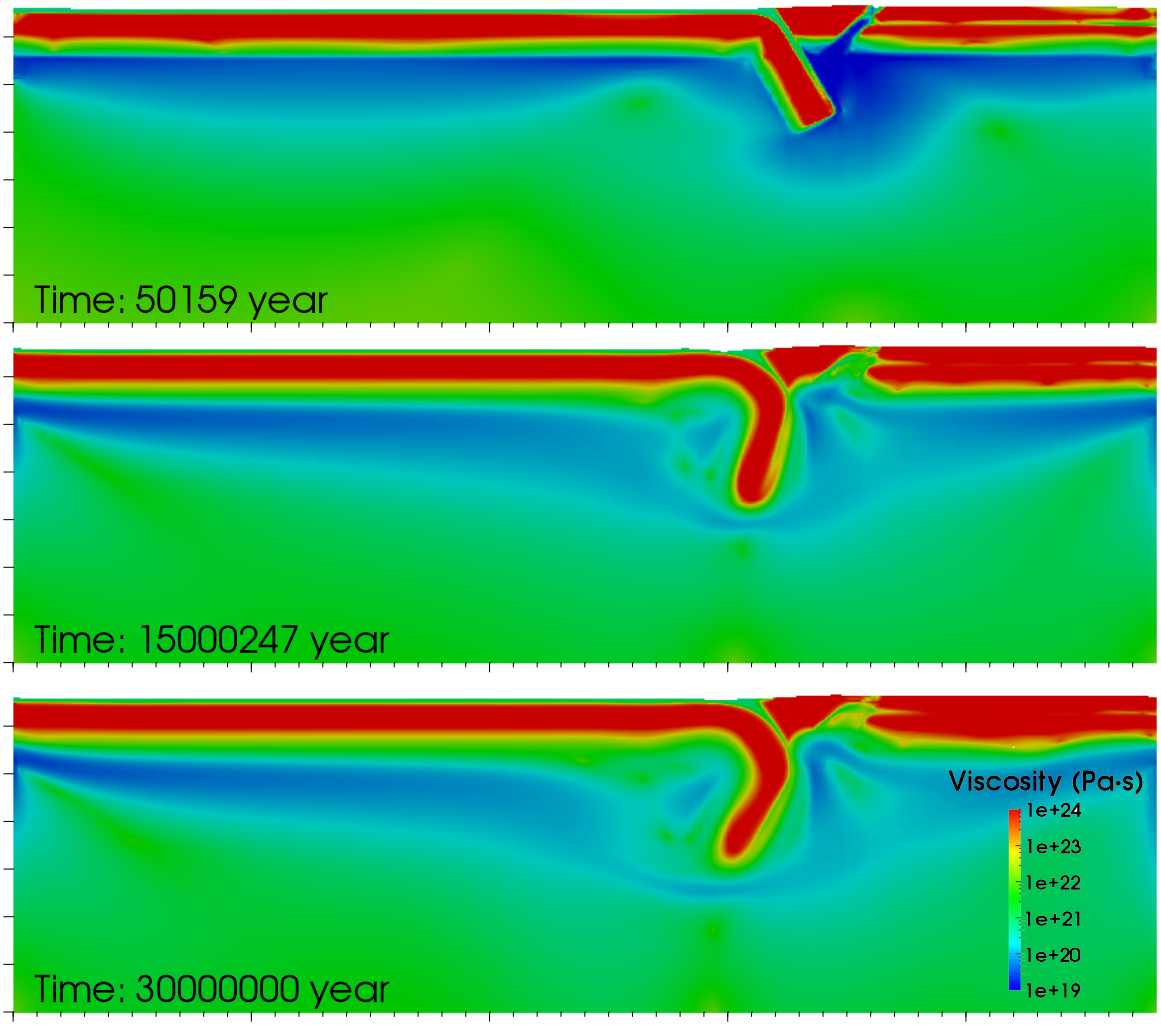

Figure 15: Evolution of a model with prescribed velocities, mantle wind a geometric averaging scheme. Locking of the system due to high viscosity in weak zone, very little rollback and back-arc extension. Curvature of the slab is caused by the mantle wind

4.2.3 Open boundaries

Contrary to the model with open boundaries and a harmonic average, this model does not include any rollback of the slab. Again, the system is locked and the viscosity in the inherited weak zone increases through time (figure 16). However, the block representing Corsica-Sardinia keeps a high viscosity, which is an improvement with respect to the model with an harmonic average. At the start of the model, the viscosity just below the lithosphere is still low, but increases rapidly if the model evolves. The slab sinks vertical and does not curve, since there is no enhancing mantle wind and the only forces acting on the slab are the convergence velocity and gravity.

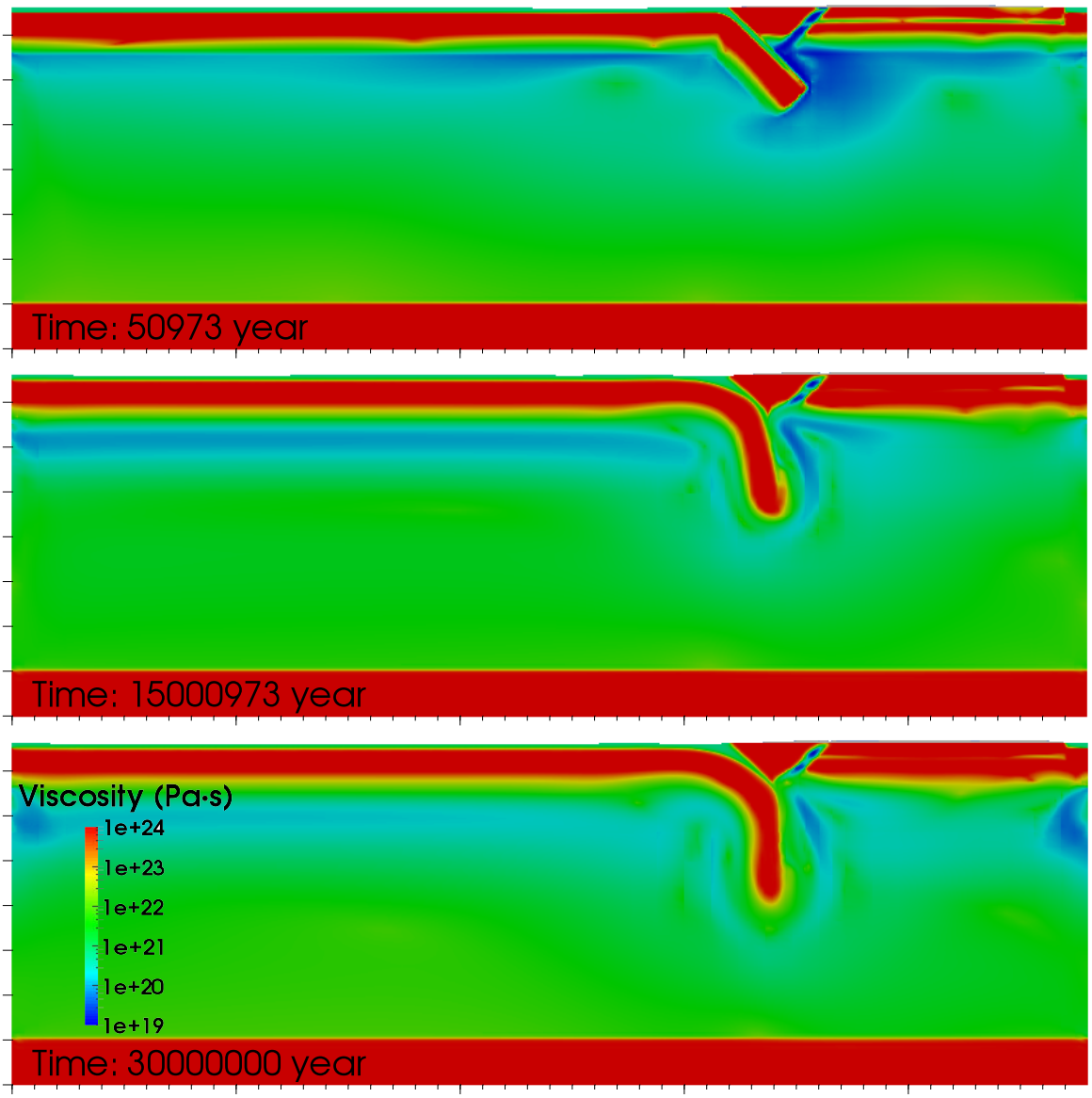

Figure 16: Evolution of a model with open boundaries from the start and a geometric averaging scheme. Locking of the system due to narrow weak zone, no rollback and back-arc extension

4.2.4 Hybrid model

The hybrid model of the geometric average with a mantle wind and prescribed boundary velocities during the first 18 My of the model run and no mantle wind and open boundaries in the second phase, shows a slightly different evolution when an extra weak zone is implemented between the slab and the Corsica-Sardinia block. The velocity of convergence of the lithospheric plates is unaffected by these boundary conditions, and can be adjusted by the user for the whole model run.

Boundary velocity variations The dependence of the rollback of the slab on the convergence velocity can be tested by varying the convergence rates that are implemented for the subducting plate crust in an equal model setup. In the models with the harmonic averaging scheme, the velocity of the incoming plate was fixed at 0.5 cm/year. For this test, the model evolutions with different convergence velocities will be tested, after a period of 18 million years where a velocity of 0.5 cm/y is used to initiate the subduction process. This convergence velocity, in combination with the mantle wind, causes the slab to sink to the 660 km discontinuity. Rollback in this hybrid model is supported by the presence of the second weak zone. After 18 million years, the slab has reached the 660 boundary, and after that the mantle wind is turned off and open boundaries are used. The weak zone between the subducting plate and the Corsica-Sardinia block proves to be necessary to prevent the model with a geometric average from locking.

Three different evolutions are evaluated: one with an increased convergence velocity of 1 cm/y as proposed by Dewey et al. (1989), one with the convergence velocity of 0.5 cm/y used in previous experiments and one with zero convergence velocity (overriding and subducting plate fixed). Figure 17 shows the evolution of the different models. To see the effects of the velocity variations clearly, the model runs are extended until 45 million years. The model with two fixed plates after 18 million years (figure 17a) shows a small trench retreat that occurs very slowly compared to the first stage of the model where the mantle wind was still on (figure 18). The second model, with a convergence velocity of 0.5 cm/year shows a trench which is almost stationary, but at larger depth the slab tip gets overturned because of the weight of the slab on top of it. The last model, with a convergence velocity of 1 cm/year for the subducting plate, shows a trench advance. This causes the slab tip to become even more curved compared to the 0.5 cm/year model. When the mantle wind is turned off, the strain rate decreases, resulting in a viscosity which increases throughout the whole model. This influences the rollback rate again, resulting in a system which is more locked. For these models with the geometric viscosity averaging scheme, the rigid Corsica-Sardinia block also does not disappear when the model evolves through time.

The model with the fixed plates and the corresponding retreating trench is the least inconsistent with the actual situation in the Western Mediterranean for the first million years of model run. However, the absolute values and the rates of trench retreat and advance which are visible in figure 18a and 18b respectively, show a trend which does not mimic the perceived setting. The total amount of trench retreat for all models is

less than 450 km, which too little if it is compared to the combined amount of rollback in the Liguro Provençal basin and the Tyrrhenian basin during the last 30 million years. The amount of rollback during the first 15 million years of model run is roughly equal to that observed in the Liguro Provençal basin, but during the second phase of the simulation the amount of rollback is severely underdeveloped compared to the actual situation as obtained from Faccenna et al. (2004) and the geometry of the slab is not correct.

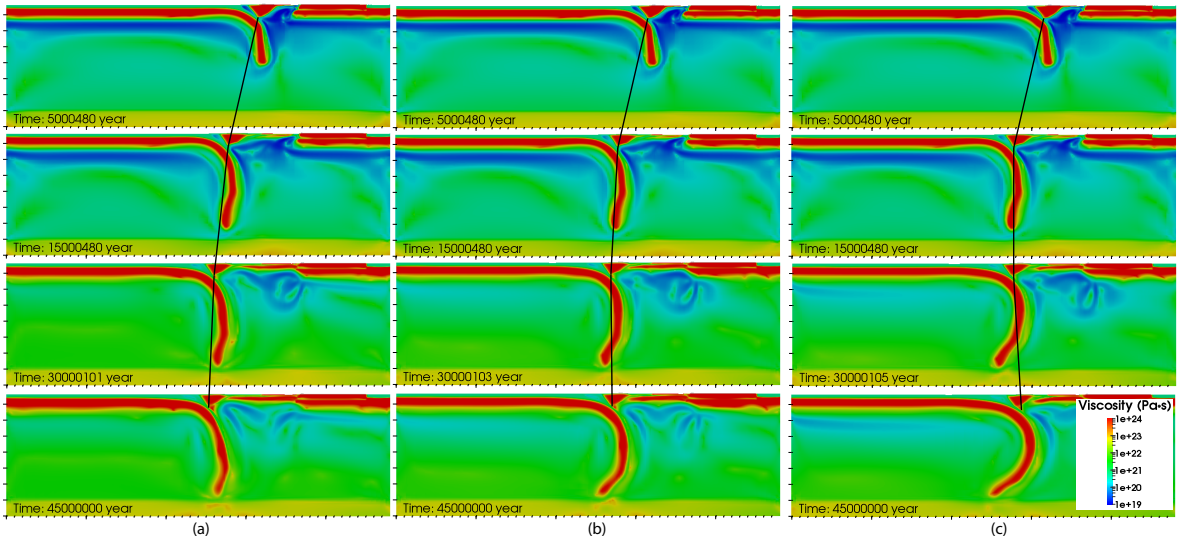

Figure 17: Model evolutions of tests with a different converging velocity after 18 million years. a) Model with stationary subducting and overriding plate ; b) Model with a fixed overriding plate, and a convergence velocity of 0.5 cm/y for the subducting plate; c) Model with a fixed overriding plate, and a convergence velocity of 1 cm/y for the subducting plate

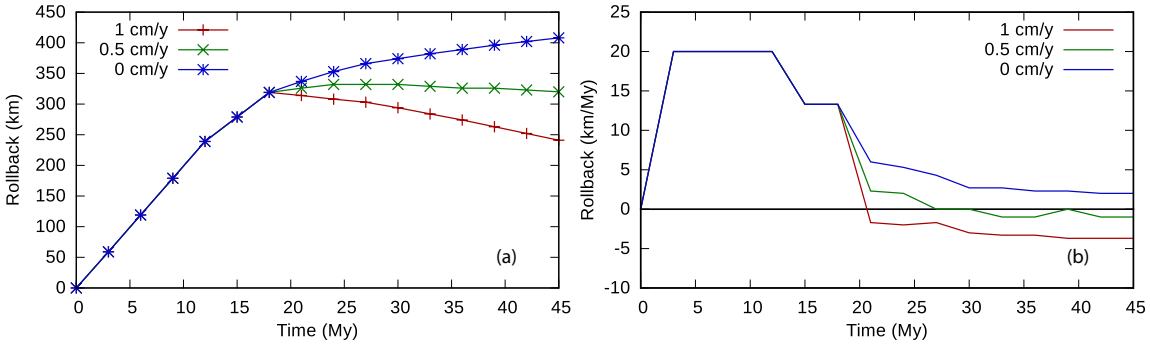

Figure 18: a) Absolute amount of rollback for the models with different convergence velocity after 18 million years ; b) Amount of rollback per million year for the different models. A positive value corresponds to trench retreat, a negative value to trench advance.

5 Discussion

5.1 Testing the Faccenna hypothesis

The main aim of the modelling experiments was to simulate the geological situation in the Western Mediterranean with 2D numerical models and to test the hypothesis regarding rollback stagnation and reactivation posed by Faccenna et al. (2001). Fine tuning of an initial set up with a combination of custom and original ASPECT plugins finally resulted in multiple different models. Whereas most models in this study indeed were able to develop a subduction zone with a sinking slab and rollback, the geometries of the different tests varied a lot depending on the boundary conditions and initial set up. The main differences were caused by the choice of the viscosity averaging scheme.

The implemented boundary conditions proved to have a large influence on the evolution of the simulations, especially for the model with an harmonic average and prescribed boundary velocities. The implementation of a mantle wind to simulate the toroidal flow is very important in increasing the steepness of the slab dip. Without the use of a mantle wind, the escape flow below the tip of the slab becomes dominant and prevents the slab from reaching the 660 discontinuity. The mantle wind supports the slab to sink more vertical, but for an harmonic average the slab still arrives at the 660 with an oblique angle, so a stronger mantle wind should be implemented. However, this forcing of increasing the steepness of the slab, as well as the use of the mantle wind after the slab tip has reached the 660, is a bit controversial. The mantle wind acts as an enhancing flow during the first stages of the model, but when the compartment behind the slab is sealed and the mantle wind is not turned off, it acts as a forced suction on the slab, which makes the rollback induced and not natural.

Adjusting the convergence velocity with the open boundaries and a geometric average also has a big influence on the evolution of the model. Dewey et al. (1989) proposed that the convergence direction of Africa with respect to Europe changed during the last 10 million years until present. This change in direction resulted in a higher convergence velocity, which in my models was tried to be simulated in the model with a convergence velocity of 1 cm per year. However, where trench retreat is the dominant motion in the Western Mediterranean, the modelled scenario showed a small advance of the trench for a geometric averaging scheme. The motion of the trench the models of figure 17 was very small in general. This indicates that the system is more locked, which is the result of higher viscosities (10^{21} compared to 10^{19}) in the mantle due to a lower strain rate. The high viscosity in the slab prevents the slab hinge from sinking further in the mantle, causing a further slowing down of the rollback process. Hence, a higher convergence rate in combination with a geometric average yields an incorrect simulation.

The total amount of rollback in the Liguro Provençal basin and the Tyrrhenian basin is estimated to be 780 km in the last 30 million years (Faccenna et al., 2004). Some models managed to obtain an amount of rollback which was almost equal to this value, especially the model with an harmonic average and open boundaries that

experienced 790 km of rollback in 30 million years. However, other models did not even reach half of the amount of rollback, or severely overestimated the rollback distance. Especially models with a geometric average failed to accommodate sufficient rollback due to locking of the subduction system, caused by a high viscosity in the subduction channel and weak zone. Only by fine-tuning the initial conditions with a mantle wind it was possible to obtain some rollback. Using open boundaries for a geometric setup never resulted in a significant amount of rollback and back-arc extension, and is therefore not an adequate model for the Western Mediterranean.

Contrary to the models with a geometric average, the models with an harmonic average were able to simulate the observed rollback, and even overshoot it for some set ups. Especially the model with an harmonic average, hybrid boundary conditions and a weak zone with very weak material between the subducting plate crust and the Corsica-Sardinia block showed an rollback amount which was significantly larger than that observed in the Western Mediterranean. Furthermore, the model showed a simultaneous extension in both weak zones next to the Corsica-Sardinia block, suggesting that the Liguro Provençal basin and the Tyrrhenian basin developed at the same time, which is not realistic. Most of the models also failed in conserving the high viscosity block representing Corsica and Sardinia, which was primarily the case for models with a harmonic viscosity averaging scheme. However, as can be seen in figure 11, a significant amount of the initial continental block composition is advected through the model.

5.1.1 Evaluation of the most promising model

The model run with an harmonic averaging scheme, open boundaries and only one weak zone in the overriding plate showed the best results regarding the amount of rollback and the final geometry of the slab. However, the distribution of rollback and back-arc extension through time does not correspond to the actual situation. Rollback rates of this model, combined with a theoretical distribution of rates as they should have been is visualized in figure 19. The red line indicates the total amount of rollback during the first 30 million years of model run, which is 790 km for this set up, as could also be derived from figure 11. The rate of rollback has not been constant during the model run. The first million years of the simulation show a relatively low rollback rate below 1 cm/yr. However, rollback rates accelerate until approximately 17 million years to 4 cm/yr. After a short stagnation of the rollback rate at 4 cm/yr, there is a small decrease to 3 cm/yr from 20 million years onwards. Hence, there is a deceleration of rollback, but no stagnation period. Furthermore, Faccenna et al. (2004) showed that there is an acceleration of rollback rate in the last few million years, corresponding to the opening of the Tyrrhenian basin. This acceleration is not present in the presented model. Hence, the model fails to accurately simulate the rollback history with the two-stage opening of the region, despite the similarities in slab geometry and amount of rollback.

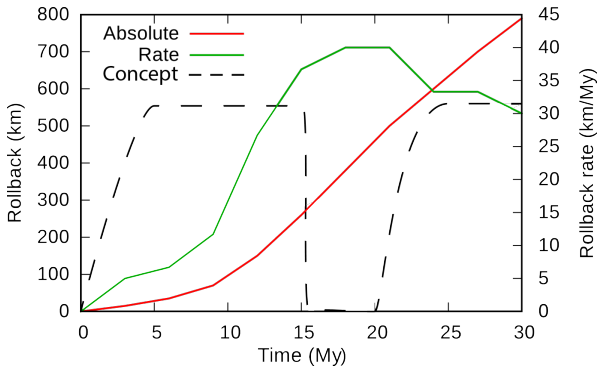

Figure 19: Evolution of rollback through time. Absolute values and rates through time are indicated with the continuous lines. The dashed line gives a conceptual representation of the stagnation and the two-stage opening of the basins

5.1.2 Strength of the weak zone material

The strength of the material in the weak zone seems to play a major role in the evolution of the overriding plate deformation. If the material in the weak zone is made 100x weaker than the original material, deformation is localizing in both this and the other weak zone. However, when the material in this weak zone between the continental block and the slab is made stronger, deformation is primarily focused in the other weak zone. From this, it becomes clear that the material properties of the overriding plate and inherited weak zones is of major importance for the development of overriding plate deformation. Even a zone which is only twice as weak as the original material already shows a different evolution. Hence, the exact strength of the material in the fault/suture zones in the Western Mediterranean should be determined.

5.2 Model improvements

All simulations performed in this study do not exactly mimic the situation as is observed in the Western Mediterranean. The 2D model runs in this study all have been performed using boundary conditions which are approximations of the real situation, assuming no external forces acting on the region except for the one resulting from Europe-Africa convergence. If further research using numerical modelling will be done in this region, there are a few model improvements that may help to simulate the geological setting of the Western Mediterranean.

5.2.1 2D vs. 3D modelling

In this study, a 2D numerical model has been performed to simulate a 3D geometry. In general, this could give a good approximation of the real situation without the costs of large computation times. However, in the case of the Western Mediterranean and especially the Calabrian slab, a 2D model might not be sufficient. The toroidal flow around the slab edges can not be modelled properly in a 2D model. The implementation of a constant mantle wind is somewhat forced due to the way it is calculated and

distributed throughout the model run. The implementation of the mantle wind can be improved by making the evolution of the amount of mantle wind dependent on depth and variable through time (i.e. no mantle wind in the bottom part of the domain when the slab is still confined to the upper part). However, finding the correct amount of mantle wind will still be a challenge. A mantle wind which is too strong will cause an overturned curvature of the slab, but a mantle wind which is too weak will cause the slab to flatten. Therefore, a 3D model including both slab edges of the Calabrian slab can better be performed to make a decent simulation of the geological history in the region. The disadvantage of such a model is that it is much more expensive in computation time for an equal resolution. The 3D model has to be set up in such a way that it includes a resolution that is high enough to visualize all geological features, but is efficient in computation time.

5.2.2 Solver type

All models performed in this study have been solved using Picard iterations, which can be relatively cheap compared to for instance Newton iterations, but convergence can be slower Paniconi and Putti (1994). The average computation time of a model run in this study was approximately 3 to 4 days for around 500000 degrees of freedom. The implementation of a Newton solver would in theory decrease this computation time, allowing for models with a higher resolution or 3D models as proposed in the previous section. The main advantage of a Newton solver is that the solver tolerances can be put less strict, which results in a decrease in absolute computation time. Both the tolerance of the linear solver and the non-linear solver can be adjusted. The Newton solver is not used in this study since it is not completely implemented in ASPECT at the moment. However, future studies should be able to use the Newton solver in ASPECT.

5.2.3 Implementation of phase transitions

Phase transitions Anderson (1967) play an important role on the density distribution in the upper mantle. The phase transition at 410 km depth causes the slab to become denser and as a result the slab pull is increased considerably (Blom, 2016). An increase in density and slab pull of the slab may cause the slab to sink more vertical, resulting in a stagnation at the 660. Blom (2016) provided a plug-in, which could be used to implement phase changes in the modelling domain.

5.2.4 Parameter variations

In this study, a certain set of parameters has been adjusted to generate different model set ups. However, there are innumerable possibilities to vary the parameter set. Varying these other parameters may yield completely different results. Future studies could for instance focus on the effect of varying the empirically determined rheological parameters, or on analyzing the far field effects of mantle flow. It might even be possible to incorporate boundary velocities from GPlates, obtained from the reconstruction of the region made by van Hinsbergen et al. (2014).

6 Conclusion

Simulating the geological history of the Western Mediterranean using a 2D numerical model has proven to be challenging. The observed pattern of episodic rollback with a stagnation period in between has not been possible to model in 2D with the used parameter set. Variations in velocity boundary conditions and strength of the overriding plate with inherited weakness alone are not sufficient to mimic the present geological setting.

Toroidal flow around the slab edges probably plays a major role in the evolution of the overriding plate deformation, and could not be modelled properly in the 2D model. Besides, the strength of the material in the weak zone controls the deformation location as well as the timing of back-arc extension. The strength ratio between the material in the weak zone and the subducting plate crust should be determined accurately to simulate the controlling factors of the opening of the Tyrrhenian basin.

The choice of the viscosity averaging scheme has a major effect on the evolution of the model. A geometric averaging scheme is able to maintain the high viscosity block representing Corsica and Sardinia, but does not give promising results regarding both amount of rollback and slab shape. An harmonic average gives a more realistic slab shape and rollback evolution, but the high viscosity continental block is affected by numerical diffusion through time and disappears partly. However, when using an harmonic average, a combination of a 3D model with a good choice of the strength of the material in the weak zone is a promising starting point for future studies to simulate the geological history and present day setting of the Western Mediterranean.

References

Advokaat, E. L., van Hinsbergen, D. J., Maffione, M., Langereis, C. G., Vissers, R. L., Cherchi, A., Schroeder, R., Madani, H., and Columbu, S. (2014). Eocene rotation of sardinia, and the paleogeography of the western mediterranean region. *Earth and Planetary Science Letters*, 401:183–195.

Alvarez, W., Cocozza, T., and Wezel, F. C. (1974). Fragmentation of the alpine orogenic belt by microplate dispersal. *Nature*, 248(5446):309.

Anderson, D. L. (1967). Phase changes in the upper mantle. *Science*, 157(3793):1165–1173.

Arndt, D., Bangerth, W., Davydov, D., Heister, T., Heltai, L., Kronbichler, M., Maier, M., Pelteret, J.-P., Turcksin, B., and Wells, D. (2017). The `deal.II` library, version 8.5. *Journal of Numerical Mathematics*, 25(3):137–146.

Bangerth, W., Dannberg, J., Gassmöller, R., Heister, T., et al. (2017). ASPECT: Advanced Solver for Problems in Earth's ConvecTion, User Manual. doi:10.6084/m9.figshare.4865333.

Berg, A. P., Keken, P. E., and Yuen, D. A. (1993). The effects of a composite non-newtonian and newtonian rheology on mantle convection. *Geophysical Journal International*, 115(1):62–78.

Blom, C. (2016). State of the art numerical subduction modelling with aspect; thermomechanically coupled viscoplastic compressible rheology, free surface, phase changes, latent heat and open sidewalls. *MSc Thesis Utrecht University*.

Boussinesq, J. (1897). *Théorie de l'écoulement tourbillonnant et tumultueux des liquides dans les lits rectilignes à grande section...*, volume 1. Gauthier-Villars.

Burrus, J. (1984). Contribution to a geodynamic synthesis of the provencal basin (north-western mediterranean). *Marine Geology*, 55(3-4):247–269.

Burstedde, C., Wilcox, L. C., and Ghattas, O. (2011). `p4est`: Scalable algorithms for parallel adaptive mesh refinement on forests of octrees. *SIAM Journal on Scientific Computing*, 33(3):1103–1133.

Chamot-Rooke, N., Gaulier, J.-M., and Jestin, F. (1999). Constraints on moho depth and crustal thickness in the liguro-provençal basin from a 3d gravity inversion: geodynamic implications. *Geological Society, London, Special Publications*, 156(1):37–61.

Dewey, J., Helman, M., Knott, S., Turco, E., and Hutton, D. (1989). Kinematics of the western mediterranean. *Geological Society, London, Special Publications*, 45(1):265–283.

Dewey, J. F., PITMAN III, W. C., Ryan, W. B., and Bonnin, J. (1973). Plate tectonics and the evolution of the alpine system. *Geological society of America bulletin*, 84(10):3137–3180.

Doglioni, C. (1991). A proposal for the kinematic modelling of w-dipping subductions-possible applications to the tyrrhenian-apennines system. *Terra Nova*, 3(4):423–434.

Doglioni, C., Gueguen, E., Sàbat, F., and Fernandez, M. (1997). The western mediterranean extensional basins and the alpine orogen. *Terra Nova*, 9(3):109–112.

Dvorkin, J., Nur, A., Mavko, G., and Ben-Avraham, Z. (1993). Narrow subducting slabs and the origin of backarc basins. *Tectonophysics*, 227(1-4):63–79.

Faccenna, C., Funiciello, F., Giardini, D., and Lucente, P. (2001). Episodic back-arc extension during restricted mantle convection in the central mediterranean. *Earth and Planetary Science Letters*, 187(1-2):105–116.

Faccenna, C., Piromallo, C., Crespo-Blanc, A., Jolivet, L., and Rossetti, F. (2004). Lateral slab deformation and the origin of the western mediterranean arcs. *Tectonics*, 23(1).

Fraters, M. (2014). Thermo mechanically coupled subduction modelling with aspect. *MSc Thesis Utrecht University*.

Gaina, C., Torsvik, T. H., van Hinsbergen, D. J., Medvedev, S., Werner, S. C., and Labails, C. (2013). The african plate: A history of oceanic crust accretion and subduction since the jurassic. *Tectonophysics*, 604:4–25.

Girod, M. and Girod, N. (1977). Contribution de la pétrologie à la connaissance de l'évolution de la méditerranée occidentale depuis l'oligocène. *Bulletin de la Société Géologique de France*, 7(3):481–488.

Gleason, G. C. and Tullis, J. (1995). A flow law for dislocation creep of quartz aggregates determined with the molten salt cell. *Tectonophysics*, 247(1-4):1–23.

Gong, Z., Langereis, C., and Mullender, T. (2008). The rotation of iberia during the aptian and the opening of the bay of biscay. *Earth and Planetary Science Letters*, 273(1-2):80–93.

Govers, R. and Wortel, M. (2005). Lithosphere tearing at step faults: Response to edges of subduction zones. *Earth and Planetary Science Letters*, 236(1-2):505–523.

Hassani, R., Jongmans, D., and Chéry, J. (1997). Study of plate deformation and stress in subduction processes using two-dimensional numerical models. *Journal of Geophysical Research: Solid Earth*, 102(B8):17951–17965.

Hawkins, J. W. (1995). The geology of the lau basin. In *Backarc Basins*, pages 63–138. Springer.

Heister, T., Dannberg, J., Gassmöller, R., and Bangerth, W. (2017). High accuracy mantle convection simulation through modern numerical methods. II: Realistic models and problems. *Geophysical Journal International*, 210(2):833–851.

Heroux, M. A., Bartlett, R. A., Howle, V. E., Hoekstra, R. J., Hu, J. J., Kolda, T. G., Lehoucq, R. B., Long, K. R., Pawlowski, R. P., Phipps, E. T., et al. (2005). An overview of the trilinos project. *ACM Transactions on Mathematical Software (TOMS)*, 31(3):397–423.

Hirth, G. and Kohlstedt, D. (2003). Rheology of the upper mantle and the mantle wedge: A view from the experimentalists. *Inside the subduction Factory*, pages 83–105.

Hirth, G. and Kohlstedt, D. L. (1996). Water in the oceanic upper mantle: implications for rheology, melt extraction and the evolution of the lithosphere. *Earth and Planetary Science Letters*, 144(1-2):93–108.

Kameyama, M., Yuen, D. A., and Karato, S.-I. (1999). Thermal-mechanical effects of low-temperature plasticity (the peierls mechanism) on the deformation of a viscoelastic shear zone. *Earth and Planetary Science Letters*, 168(1-2):159–172.

Karato, S.-i. and Wu, P. (1993). Rheology of the upper mantle: A synthesis. *Science*, 260(5109):771–778.

Kaus, B. J., Mühlhaus, H., and May, D. A. (2010). A stabilization algorithm for geodynamic numerical simulations with a free surface. *Physics of the Earth and Planetary Interiors*, 181(1-2):12–20.

Kley, J. and Voigt, T. (2008). Late cretaceous intraplate thrusting in central europe: Effect of africa-iberia-europe convergence, not alpine collision. *Geology*, 36(11):839–842.

Kronbichler, M., Heister, T., and Bangerth, W. (2012). High accuracy mantle convection simulation through modern numerical methods. *Geophysical Journal International*, 191(1):12–29.

Lacombe, O. and Jolivet, L. (2005). Structural and kinematic relationships between corsica and the pyrenees-provence domain at the time of the pyrenean orogeny. *Tectonics*, 24(1).

Lustrino, M., Morra, V., Fedele, L., and Franciosi, L. (2009). Beginning of the apennine subduction system in central western mediterranean: constraints from cenozoic "orogenic" magmatic activity of sardinia, italy. *Tectonics*, 28(5).

Malinverno, A. and Ryan, W. B. (1986). Extension in the tyrrhenian sea and shortening in the apennines as result of arc migration driven by sinking of the lithosphere. *Tectonics*, 5(2):227–245.

Mantovani, E., Albarello, D., Tamburelli, C., and Babbucci, D. (1996). Evolution of the tyrrhenian basin and surrounding regions as a result of the africa-eurasia convergence. *Journal of Geodynamics*, 21(1):35–72.

McKenzie, D. (1970). Temperature and potential temperature beneath island arcs. *Tectonophysics*, 10(1-3):357–366.

Montigny, R., Edel, J., and Thuizat, R. (1981). Oligo-miocene rotation of sardinia: Kar ages and paleomagnetic data of tertiary volcanics. *Earth and Planetary Science Letters*, 54(2):261–271.

Morra, G. (2015). *Subduction dynamics: From mantle flow to mega disasters*. John Wiley & Sons.

Paniconi, C. and Putti, M. (1994). A comparison of picard and newton iteration in the numerical solution of multidimensional variably saturated flow problems. *Water Resources Research*, 30(12):3357–3374.

Rehault, J.-P., Boillot, G., and Mauffret, A. (1984). The western mediterranean basin geological evolution. *Marine Geology*, 55(3-4):447–477.

Rose, I., Buffett, B., and Heister, T. (2017). Stability and accuracy of free surface time integration in viscous flows. *Physics of the Earth and Planetary Interiors*, 262:90–100.

Rosenbaum, G. and Lister, G. S. (2004). Neogene and quaternary rollback evolution of the tyrrhenian sea, the apennines, and the sicilian maghrebides. *Tectonics*, 23(1).

Rosenbaum, G., Lister, G. S., and Duboz, C. (2002a). Relative motions of africa, iberia and europe during alpine orogeny. *Tectonophysics*, 359(1-2):117–129.

Rosenbaum, G., Lister, G. S., Duboz, C., et al. (2002b). Reconstruction of the tectonic evolution of the western mediterranean since the oligocene. *Journal of the Virtual Explorer*, 8:107–130.

Sartori, R. et al. (1990). The main results of odp leg 107 in the frame of neogene to recent geology of perityrrhenian areas. In *Proc. Ocean Drill. Program Sci. Results*, volume 107, pages 715–730.

Seno, T. and Maruyama, S. (1984). Paleogeographic reconstruction and origin of the philippine sea. *Tectonophysics*, 102(1-4):53–84.

Séranne, M. (1999). The gulf of lion continental margin (nw mediterranean) revisited by ibs: an overview. *Geological Society, London, Special Publications*, 156(1):15–36.

Spakman, W. and Wortel, R. (2004). A tomographic view on western mediterranean geodynamics. In *The TRANSMED atlas. The Mediterranean region from crust to mantle*, pages 31–52. Springer.

Stampfli, G., Borel, G. D., Marchant, R., and Mosar, J. (2002). Western alps geological constraints on western tethyan reconstructions. *Journal of the Virtual Explorer*, 8:77.

van Hinsbergen, D. J., Vissers, R. L., and Spakman, W. (2014). Origin and consequences of western mediterranean subduction, rollback, and slab segmentation. *Tectonics*, 33(4):393–419.

Vissers, R. and Meijer, P. T. (2012). Mesozoic rotation of iberia: subduction in the pyrenees? *Earth-Science Reviews*, 110(1-4):93–110.

Wortel, M. and Spakman, W. (2000). Subduction and slab detachment in the mediterranean-carpathian region. *Science*, 290(5498):1910–1917.